Biomass-mapping of alpine grassland with APEX imaging spectrometry data

MSc Thesis

Zur Erlangung des Grades

MSc UNIGIS

der Universität Salzburg

vorgelegt von

Maja Rapp

U1509

Eingereicht am 30.03.2013

EIDESSTATTLICHE ERKLÄRUNG

Ich erkläre hiermit an Eides statt, dass ich die vorliegende Thesis selbständig und ohne unzulässige fremde Hilfe angefertigt habe. Die verwendeten Quellen sind vollständig zitiert.

Datum: 30.03.2013 Unterschrift:

ABSTRACT

Today remote sensing is a standard technique for mapping land cover in high spatial resolution over large areas. Not only land cover but also the quality and quantity of vegetation can be classified by the analysis of imaging spectroscopy data. In the Swiss National Park (SNP) we use data from the Airborne Prism Experiment (APEX) imaging spectrometer to expand the possibilities of vegetation analysis in alpine territories. The high spectral and spatial resolution of APEX data allows the correlation of the measured reflection with ground truth data.

In this work a standard Normalized Differenced Vegetation Index (NDVI) and an optimized simple ratio index (SRI) with selected bands were generated to model the biomass content of the alpine grassland of one particular valley in the SNP, the Val Trupchun.

The correlation between biomass *insitu* measurements and SRIs was non-linear, most likely due to sensor saturation. Our optimal SRI improved the model quality compared to the NDVI model. All computed models underestimated high biomass values above 600 g/m^2. The model accuracy of 57% was good considering the challenging terrain. However, several factors showed that the model was relatively unstable due to parameter input settings and external factors. Differences in APEX data between strips induced an important effect, due to different illumination/view angles. The variability analysis investigating the sample plot location demonstrated that small-scale geometrical shifts were insignificant compared to the overall model accuracy. The biomass prediction map showed plausible values for the grassland with high concentrations around former alps. High biomass sources were linked to former anthropogenic land use, dominant vegetation structure and to preferred ungulate habitat today.

The high-resolution map is now a useful basis for future research in the SNP to investigate forage amount and analyse ungulate habitat pattern in Val Trupchun. This a

welcoming issue for ungulate research, which is an important research area of the SNP.

TABLE OF CONTENTS

LIST OF FIGURES

LIST OF TABLES

ACKNOWLEDGEMENTS

An dieser Stelle bedanke ich mich bei allen, die mir bei dieser Arbeit geholfen, mich unterstützt und zum Gelingen beigetragen haben. Ein besonderer Dank gilt Anna Schweiger vom SNP für die fachliche und moralische Unterstützung, Alexander Damm vom RSL für seine Bemühungen und fachliche Hilfe als Experte, Pia Anderwald für die umfassende englische Korrektur, Antonia Eisenhut für die kartographische Unterstützung, Ruedi Haller für die Geduld und das Verlängern der Anstellung und dem gesamten SNP Team für die Freude bei der Arbeit. Des Weiteren ist Mathias Kneubühler zu nennen, der wesentlich zur Themenfindung der Arbeit beigetragen hat und dem gesamten UNIGIS-Team für die gute Betreuung während des Studiums.

1 INTRODUCTION

Imaging spectrometry or imaging spectroscopy is a remote sensing technique recording the earth's surface by a hyperspectral sensor. The technique was developed in the early 1980s and 1990s (Goetz et al., 1985; Vane et al. 1984) and started with airborne instruments. Several airborne imaging spectrometers have been developed so far such as the hyperspectral scanner HyMAP by HyVista, Airborne Visible/Infrared Imaging Spectrometer AVIRIS by NASA, Airborne Imaging Spectrometer for Application AISA by Specim Ltd. and Airborne Prism Experiment APEX by ESA. The first imaging spectrometer was launched in space by NASA's Moderate-resolution Imaging Spectroradiometer MODIS in 1999.

Imaging spectrometers have been used successfully to create maps that consist of land cover units with discernible spectral differences in the sensor's band set. The sensor collects the reflectance spectra of the earth's surface induced by sunlight in many small, contiguous spectral bands (Goetz, 2009). With increased number of spectral bands and increased spatial resolution the technique now allows not only the mapping of land cover types but also the mapping of vegetation quality and quantity. Hyperspectral data have been used in ecological and vegetation studies analysing the chemical composition of plants or mapping at species level (Xiao, et al., 2004; Mutanga et al., 2004). These applications are of great interest for ecologists analysing vegetation in difficult terrain.

The Swiss National Park (SNP) was mapped by APEX (Airborne Prism Experiment) for the first time in June 2010. Land cover mapping and monitoring of landscape dynamics are essential for the management of protected areas. Since ungulate research plays an important role in the SNP, the application possibilities of the APEX data are of great interest. The SNP is inhabited by large populations of alpine ibex *(Capra ibex,* L.*)*, chamois *(Rupicapra rupicapra,* L.*)* and red deer *(Cervus elaphus,* L.*)*. The evaluation of

vegetation quantity and quality can provide important information on forage abundance and its spatial distribution. A water content map of the valley of Trupchun (Val Trupchun) has already been produced using APEX data (Kneubühler, 2011). The mapping of biomass content of the grassland serves as an additional valuable input feature for the investigation of ungulate habitat patterns.

1.1 MOTIVATION

The high alpine territory of the SNP is challenging for vegetation analysis. As field sampling is difficult and time consuming due to the hard accessibility of the terrain, traditional field research is limited. Not only are time and accessibility restricted, but the personnel effort in the field would also require substantial financial resources. Furthermore, reliable estimates are restricted to local scales only, whereas ecologists require estimates at landscape scale. Remote sensing is therefore a great technique for an area-wide interpretation of vegetation at high spatial resolution.

Ungulate research has a long tradition in the SNP and therefore the analysis of vegetation quality and quantity is an essential issue. Because ungulates need to spend most of their time grazing, the (local) composition of forage can explain their spatial distribution (Van Langenvelde & Prins, 2008). Together with other vegetation parameters such as water, nutrition and fibre content, the biomass model serves as a valuable input for the analysis of ungulate habitat and movement patterns.

1.2 OBJECTIVE

The aim of this MSc thesis is to generate a biomass map of the grassland of one particular valley of the SNP (Val Trupchun) with APEX imaging spectrometry data from June 2010. A semi-empirical method is implemented in the modelling process. First, a standard normalized-differenced-vegetation-index (NDVI) is calculated and compared with *insitu* biomass samples. To achieve a better model, a large number of simple ratio vegetation indices (SRI) are developed from the hyperspectral data and regressed against the ground truth data. Model validation is carried out by independent sample plots. The best model is taken to predict the grassland biomass in Val Trupchun.

The produced biomass map is analysed for plausibility relating to the former land use of the Val Trupchun. Furthermore the model is tested for stability and accuracy by investigating the APEX data at the overlapping zones of the different strips and analysed by the variability of the sample plot locations. A comprehensive discussion is carried out to analyse the modelling approach for accuracy, uncertainty and possibilities for improvement.

The study area of Val Trupchun was chosen due to its substantial cover of grassland and high population of ungulates. Imaging spectroscopy induces a large data volume and therefore the handling has its limitations. The whole territory of the park would be unfeasible for this modelling approach. As the territory is complex and variable at fine spatial scales, many *insitu* samples are required to obtain a useful and satisfactory prediction model. Therefore the method used here not only requires strong computing power but also substantial effort in the field.

1.3 METHODOLOGY

The APEX data is provided geometrically, atmospherically and radiometrically corrected by the Remote Sensing Laboratory of the University of Zurich (RSL) using the standard procedures ATCOR-4 (Schläpfer & Richter, 2002) and PARGE (Schläpfer & Richter, 2002). A semi-empirical modelling approach is carried out to obtain the biomass prediction map. Different model settings are tested to optimise model accuracy. The detailed methodology of pixel-based modelling of the biomass map is explained in chapter 3.

For data preparation and modelling the software ENVI 4.7 (Environment for Visualisation of Images) in combination with IDL (Interactive Data Language) by ITT VIS was used. For the cartography and simple GIS analysis the software ArcGIS 10.0 by ESRI was applied.

1.4 STRUCTURE

This MSc thesis has been carried out at the Swiss National Park in collaboration with the Remote Sensing Laboratories of the University of Zurich (RSL).

In the first chapter, an introduction to imaging spectrometry and background information about the Swiss National Park, the Valley of Trupchun and the APEX project is given. Chapter 3 explains the methodology of the modelling approach. In chapter 4, the results are presented, first the model variables and then the resulting prediction map. Furthermore results related to the model stability, accuracy and saturation are shown. The results are discussed in chapter 5. Different model parameters are reviewed here and a comprehensive uncertainty analysis is carried out. Finally, conclusions are derived from the study and an outlook to further potential studies is provided.

2 BACKGROUND

Due to their high spectral and spatial resolution, image spectrometers serve many applications over a broad range of scientific fields such as e.g. in ecology, limnology, geology, atmospheric sciences, natural hazard and disaster management, and materials detection. Application examples are mapping of soil composition, total suspended matter in lakes, plant pigments and non-pigments (water, protein, chlorophyll, lignin, cellulose, nitrogen, etc.), vegetation structure, hydrocarbon content, net and gross primary production, aerosol concentration and atmospheric water vapour. The technique is therefore a valuable tool in the management of nature parks.

2.1 RESEARCH IN THE SWISS NATIONAL PARK

The Swiss National Park (SNP) was founded in 1914 as a strict nature reserve and is the oldest national park in the Alps. The park is situated in the canton of Graubünden covering an area of 170 km^2, which is the largest protected area in Switzerland. It is the country's only national park and is classified as a category I nature reserve (highest protection level - strict nature reserve /wilderness area) with the IUCN (International Union for the Conservation of Nature). The territory encompasses an alpine landscape extending over altitudes between about 1400 to 3200 meters above sea level (asl.) with a rich flora and fauna. Research is one official mission of the park so that the territory is available for the analysis of natural processes and ecosystems in the absence of human influence. Scientists from various research institutes use this open-air laboratory to gain further knowledge of alpine species and habitats. Minimal human disturbance and the availability of results from earlier projects carried out during many years offer ideal conditions for a variety of research activities.

As ecological and ungulate research have a long tradition in the SNP, many valuable long-term data series and publications are available. Since 1917, the vegetation has been monitored on more than 150 permanent plots (Braun-Blanquet et al., 1931;

Stüssi, 1970). In 1968 an analogue vegetation map of part of the SNP was produced in cartography work by Trepp/Campell at a scale of 1:10'000 (Trepp & Campbell, 1968). In 1992, Zoller published a vegetation map of the entire SNP (Zoller, 1992). It was based on observation plots and field trips, and mapped at a 1:50'000 scale. An interpretation of colour infra-red aerial images was conducted over the whole territory of the SNP as part of the project Alpine Habitat Diversity (HABITALP[1]) in 2006. A common coded interpretation key was developed to map area-wide standardized delimitation of land use types at a 1:5'000 scale. The interpretation allowed not only the classification of the habitats, but also assignment of the dominant vegetation species.

Until now, vegetation mapping has been based on the interpretation of single plots and visual observations, which enables only limited interpolations over large areas. The HABITALP project has been the first study with a standardized method to classify vegetation types area-wide from aerial images. Not only is a classification of habitat types possible with the APEX data, but also pixel-based modelling of vegetation composition at a scale of 2 x 2 meters.

Ungulate research in the National Park also has a long history. The SNP is inhabited by large populations of alpine ibex *(Capra ibex,* L.*)*, chamois *(Rupicapra rupicapra,* L.*)* and red deer *(Cervus elaphus,* L.*)*. Population counts have been carried out since the 1920's. Extensive ungulate projects began in the 1990's. With the assistance of telemetry and GPS radio collaring, the movement of individual animals can be recorded and graphically represented. Results from ungulate counts and GIS movement tracks in combination with vegetation studies will provide information regarding the forage availability and migration patterns of ungulate populations.

Despite the 100 years of protection, traces from the former land use can still be found on subalpine and alpine grassland. Cattle and sheep grazed the territory of the SNP for

[1] HABITALP – Alpine Habitat Diversity Project. INTERREG III B Alpenraumprogramm 2002-2006, http://habitalp.de, (last accessed on 20.03.2013)

several centuries until 1914 (Parolini, 1995). As a result, tall-herb communities dependent on nutrient enrichment from the excreta of cattle or sheep can still be found on several former pastures in the SNP (Braun-Blanquet, 1931; Braun-Blanquet et al., 1954; Pictet, 1942; Stüssi, 1970; Krüsi et al., 1995; Achermann et al., 2000).

2.2 IMAGING SPECTROSCOPY OF VEGETATION

Imaging spectroscopy is similar to colour photography, but the spectrometer acquires for each pixel many bands of light intensity data from the spectrum, instead of just the three bands of the RGB model. The sensor collects simultaneously spatially coregistered images in many spectrally contiguous bands.

The term hyperspectral imaging is often used interchangeably with imaging spectroscopy. Due to its heavy use in military related applications, the civil world has developed a slight preference for using the term imaging spectroscopy[2].

Imaging spectrometers such as APEX sample contiguously in the optical part of the electromagnetic spectrum using dozens to hundreds of narrow spectral bands. For each image pixel, the sensor acquires the reflectance of the earth's surface from the ultraviolet through the visible to the near- and mid-infrared (i.e. 250 - 2500 nm) part of the electromagnetic spectrum at a high spatial resolution. The data allows the analysis of useful and precise quantitative information about the environment. In Figure 1, a schematic of the function of imaging spectrometry is illustrated.

[2] From Wikipedia, Imaging spectroscopy. http://en.wikipedia.org/wiki/Imaging_spectroscopy, last accessed on 20.03.2013

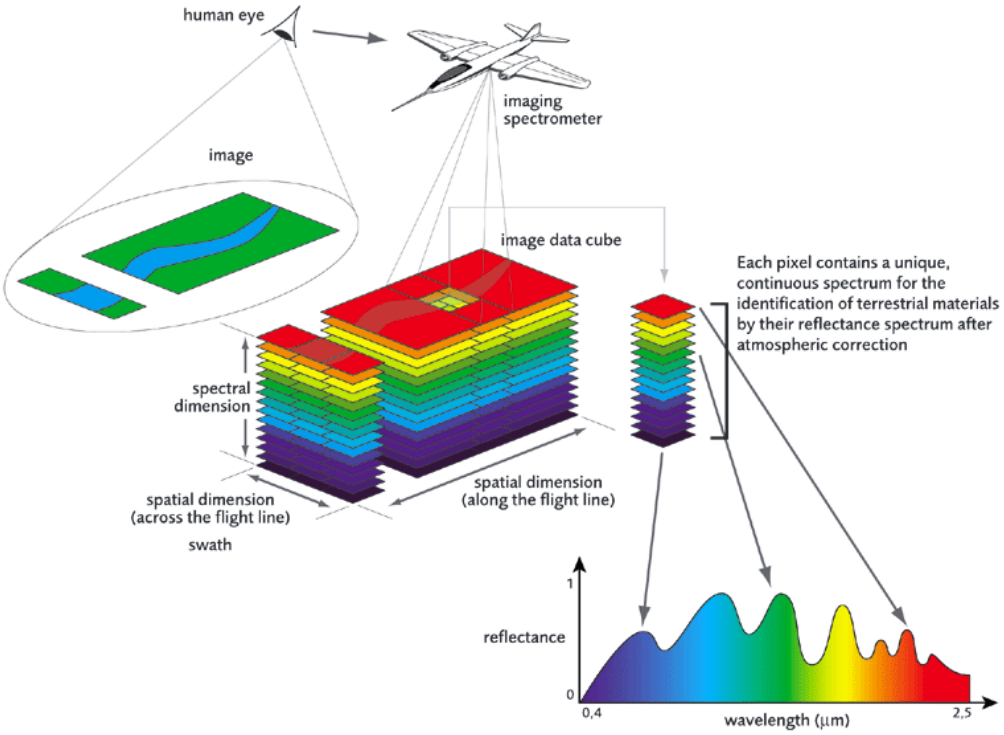

Figure 1: Working schematic of imaging spectroscopy (Image: www.apex-esa.org, last accessed 20.03.2013)

Analysing the vegetation using remotely sensed data requires knowledge of the biochemical, structural and functional vegetation characteristics and its optical properties. Vegetation interacts with solar radiation differently from other natural materials, such as soils and water bodies. Vegetation optical properties in terms of absorbing, reflecting and transmitting solar radiation is the result of many interactions with different plant materials, which varies considerably with wavelength. The interaction of radiation with plant leaves in terms of reflection, absorption and transmission depends not only on the wavelength, but also on a range of structural and chemical characteristics such as chemical composition, leaf age, leaf thickness, leave structure and water content. The wavelengths cause electronic transitions in the atoms and molecules and transfer them into molecular vibrations (rotation, bending and stretching) between the C-H, N-H, O-H, C-N and C-C bonds, which are the primary constituents of plant tissue (Mutanga, 2004). The radiation are either emitted or absorbed at distinct wavelength.

Water, pigments, nutrients and carbon are each expressed in the reflected optical spectrum from 400 nm to 2500 nm, with often overlapping, but spectrally distinct, reflectance behaviours. The absorption characteristics of these compounds determine the optical properties, which as a result are then visible in e.g. the reflectance spectra. These known signatures allow scientists to combine reflectance measurements at different wavelengths to enhance specific vegetation characteristics[3].

The typical characteristics of healthy green vegetation over the wavelength range from 400-2500 nm are shown in Figure 2. The optical spectrum is divided into four distinct wavelength regions (Lillesand & Kiefer, 1994):

1. Visible: 400 nm - 700 nm
    a. Blue: 400 - 500 nm
    b. Green: 500 - 600 nm
    c. Red: 600 - 700 nm
2. Near-infrared (NIR): 700 nm - 1300 nm
3. Shortwave infrared 2 (SWIR-1): 1300 nm - 1900 nm
4. Shortwave infrared 2 (SWIR-2): 1900 nm - 2500 nm

[3] From ENVI User's Guide: Vegetation Indices. http://geol.hu/data/online_help/Understanding_Vegetation_and_Its_Reflectance_Properties.html, last accessed on 20.03.2013.

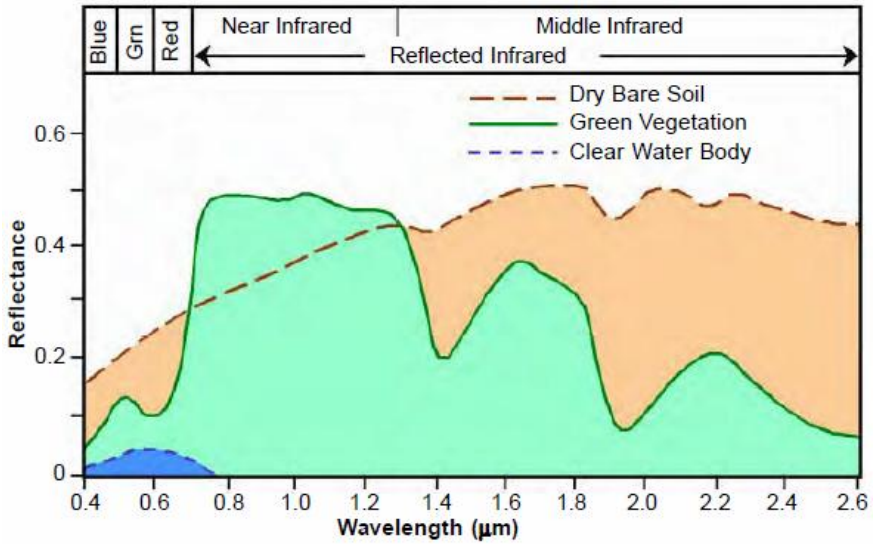

Figure 2: Typical spectral signature of vegetation, water and bare soil (Image: Remote Sensing, fundamental Concepts, from http://www.remote-sensing.net, last accessed on 06.12.2012).

The break-down from NIR to SWIR-1 is marked by the atmospheric water absorption region (around 1500 nm) in which sensors can't acquire measurements. The same occurs at the transition between SWIR-1 and SWIR-2 at 1900 nm. The sharp increase in the reflectance between the red visible (600 nm) and the NIR (800 nm) is called the red edge, a region that marks the boundary between absorption by chlorophyll in the red and scattering due to leaf internal structure in the NIR region. Increasing chlorophyll concentration results in a broadening of the chlorophyll absorption peak that moves the red edge to longer wavelengths while losses of chlorophyll as in senescence lead to shorter wavelengths for the red edge position (Jones & Vaughan, 2010).

As mentioned above the photosynthetic active chlorophyll pigments have the most influence in the signal. Other leaf pigments such as carotenoids and anthocyanins, are responsible for the autumn leaf colour, also contribute a small part of the reflection in the visible range. At the red-edge the reflectance is strongly correlated with plant biochemical and biophysical parameters (Mutanga & Skidmore, 2007; Clevers, 1999). In the NIR, there is high reflectance and transmittance, and very low absorption. The physical control is the internal leaf structure (Kumar et al., 2001; Rosso et al., 2005). In the mid-infrared there is lower reflectance than in other spectral regions due to strong water absorption and minor absorption of biochemical content (Kumar et al., 2001). Here the reflectance receives contributions from nitrogen and various forms of carbon.

The reflectance properties at canopy level depend on both individual components of the vegetation (leaves, stems, soils, water, etc.) and the canopy architecture. Additionally, the scattering and absorption inside the canopy plays an important role. Different vegetation types, e.g. forests, grasslands, or agricultural crops have different reflectance properties, even though the properties of individual leaves are usually quite similar (Jones & Vaughan, 2010). Vegetation with mostly vertical foliage such as grass reflects differently from foliage with more horizontally-oriented leaves such as trees. The most important characteristics of canopies are the leaf area index (LAI) and the leaf angle distribution (LAD). The LAI defines the leaf area per unit ground area that represents the total amount of green vegetation present in the canopy (Campbell & Norman, 1998). The LAI has the strongest effect on overall canopy reflectance. The LAD describes the overall variety of directions in which the leaves are oriented, but is often simplified by specifying the mean leaf angle (MLA), which represents the actual distribution. The MLA is the average of the differences between the angle of each leaf in a canopy and horizontal (Falster & Westoby, 2003). Whereas vegetation strongly reflects light in the NIR portion of the spectrum, canopies strongly absorb photons in the visible and SWIR-2 ranges. This induces a smaller transmission into the canopy at these wavelengths. Therefore, vegetation indices using spectral data from the visible and SWIR-2 are very sensitive to upper canopy conditions. In contrast, photons are scattered in the near-infrared and SWIR-1 range. Hence, these photons measured by an instrument come from reflections throughout much of a vegetation canopy3. The reflectance behaviour with different LAI and MLA can be seen in Figure 3.

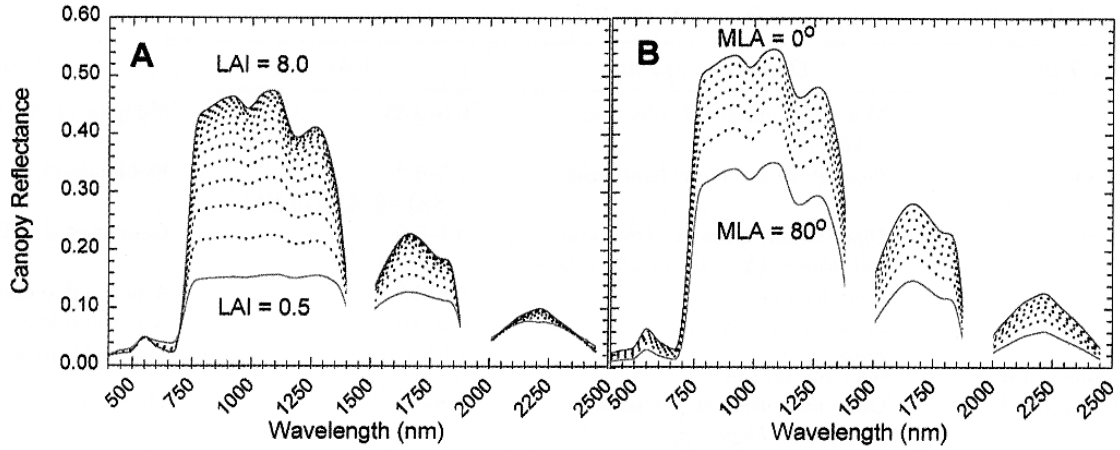

Figure 3: Canopy reflectance effects dependant with different LAI and MLA (Image: ENVI user guide, http://geol.hu/data/online_help/Understanding_Vegetation_and_Its_Reflectance_Properties.html#wp1159169, last accessed on 20.03.2013)

When analysing mixed ecosystems such as grasslands, not only the live, green vegetation, but also the dead vegetation (non-photosynthetic vegetation (NPV)) has to be considered. NPV material is composed mainly of the carbon-based molecules lignin, cellulose and starch, and the reflectance signatures are characterized by these components. Photons in the visible wavelength region are generally efficiently absorbed by live, green vegetation, and in the SWIR-2 region of the spectrum, photons are efficiently absorbed by the water content. On the other hand, the NPV scatters photons very efficiently throughout the spectrum with the most scattering occurring in the SWIR-1 and SWIR-2 ranges. The change in canopy reflectance due to increasing fractional amounts of NPV is shown in Figure 4.

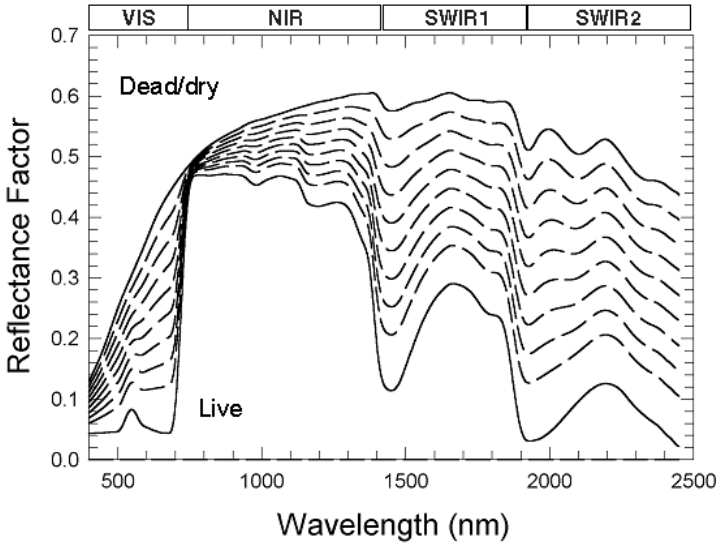

Figure 4: Changes in reflectance between dead and dry vegetation across the optical spectrum (Image: ENVI user guide, http://geol.hu/data/online_help/Understanding_Vegetation_and_Its_Reflectance_Properties.html#wp1159169, last accessed on 20.03.2013).

2.2.2 SPECTRAL INDICES

As different materials have characteristic spectra with maxima or minima at particular wavelengths, there is often no need for complex physical models to determine key biophysical parameters. Spectral indices based on empirical or semi-empirical models are new variables generated by mathematical combination of two or more of the original spectral bands chosen in such a way that the new indices are related to the biophysical parameters of interest. Especially in the use of vegetation indices (VIs), spectral indices have been widely adopted for studying vegetation cover, chlorophyll content or quantifying other vegetation properties. VIs are usually dimensionless and indicate the amount of green vegetation. A variety of VIs have been published. The best known are the Normalised Differenced Vegetation Index (NDVI, Rouse et al., 1974; Tucker, 1979), the Simple Ratio Index (SRI, Birth and McVey, 1968; Rouse et al., 1974; Tucker, 1979) and the Red Edge Position Index (REPI, Jago et al., 1999). Most vegetation indices are based on the sharp increase in reflectance from vegetation that occurs around 700 nm (the red edge), a change that is characteristic of green vegetation and absent in most other natural surfaces.

The NDVI is typically used for modelling simply and quickly the healthy green vegetation and its condition and is scaled between 0 and 1. This index is originally

introduced by Rouse et al. (1974) in order to separate green vegetation from its background soil brightness using Landsat MSS digital data. Today it is also used to quantify the photosynthetic capacity of plant canopies. It is expressed as the difference between the near infrared and red bands normalized by the sum of those bands. It retains the ability to minimize topographic effects while producing a linear measurement scale.

The SRI has the same field of application and is calculated by simply dividing the reflectance values of the near infrared band by those of the red band. The contrast between the red and infrared bands clearly results, with high index values being produced by combinations of low red (because of absorption by chlorophyll) and high infrared (as a result of leaf structure) reflectance (Birth & McVey, 1968). Because of the ratio problems of variable illumination as a result of topography are minimized to some extent.

The REPI is a narrowband reflectance measurement that is sensitive to changes in chlorophyll content. Increased chlorophyll concentration broadens the absorption feature and moves the red edge to longer wavelengths. This index is commonly used for crop monitoring, yield prediction, photosynthesis modelling or canopy stress.

With the advent of imaging spectroscopy and the availability of the large amount of narrow spectral bands, vegetation indices can be individually designed for a specific vegetation property and a specific territory. By correlating the results of the VIs with on site field data, the optimal VI is chosen to model the desired vegetation property. The advantage of the index implementing two to many bands is to minimize the sensitivity to irradiance, illumination and to other factors such as variation in atmospheric transmission. The disadvantage of empirical models and VIs is that the structural property of the vegetation can’t be modelled. Especially for dense canopies (high biomass) the VI have its limitations due to saturation.

2.2.3 State of the art in biomass estimation using VIs

The quantification of vegetation parameters is an important task in climate and ecosystem research, biomass production (food, fibre and fuel) and when investigating

land-atmosphere interactions. Accurate characterization of vegetation properties and temporal dynamics are therefore needed for many land-cover models that are used as prediction maps. These maps can provide detailed spatial information on biomass distribution which is useful in the management of protected areas, research of animal distributions and grazing effects, ecological process and habitat modelling, and when studying the effects of natural and man-made disturbances.

Grasslands belong to the earth's most wide-spread land cover types and represent the forage source for livestock and wild herbivores (Mutanga & Skidmore, 2004). Studies using hyperspectral data to estimate biomass by relating field data to vegetation indices have been carried out under controlled laboratory conditions (Mutanga & Skidmore, 2004). The biomass production of mixed grassland ecosystems under natural conditions has been investigated in several studies using hyperspectral data (Rahman & Gamon, 2004; Mirik et al., 2005; Tarr et al., 2005; Beeri et al., 2007; Cho et al., 2007; Psomas et al., 2009). These studies show the complexity of the spectral response of mixed grasslands, especially in the presence of a high fraction of NPV and exposed soil (Beeri et al., 2007; He et al., 2006; Boschetti et al., 2007), grazing impact (Numata et al., 2007), and canopy architecture complexity due to mixed species composition and phenology (Cho et al., 2007; Numata et al., 2008). Mirik (2005) estimated total and live biomass with hyperspectral 1-m resolution data by SRI and NDVI indices. The SRI or NDVI with the best relationships for biomass were found in the NIR part of the spectrum for band 1 and the visible part of the spectrum for Bands 2 with an R^2 = 0.88. Beeri et al. (2007) also estimated forage quantity and quality using hyperspectral imagery for northern mixed-grass prairie. A narrow band NDVI (802 nm, 673 nm) was calculated from HyMap imagery and regressed against ground truth data resulting in an R^2 = 0.78. Cho et al. (2007) also showed an estimation of green grass/herb biomass from airborne hyperspectral imagery using spectral indices. The NDVI and REPI were calculated from HyMap data and correlated with ground truth samples. NDVIs involving far red-edge bands in the 725 - 800 nm range produced higher coefficients compared with traditional NDVIs computed from red and NIR bands. Another study showed that narrow-band NDVI resulted in the best models to

predict aboveground biomass of dry grassland sites by field spectroradiometer (Psomas et al., 2009).

Using grass (*Cenchrus ciliaris*) grown in the greenhouse, Mutanga & Skidmore (2004) showed that narrow-band NDVI computed from 740 and 755 nm (both in the far RED) solved the saturation problem when estimating grass biomass at high canopy cover. The NDVIs of all possible band combinations were calculated and compared to the standard NDVI.

Identification of hyperspectral vegetation indices for pasture characterization has been analysed by calculating SRIs and NDVIs using all combinations of bands and regressing them against field data (Fava et al., 2009). SRIs involving bands in NIR (770 - 930 nm) and in the red edge (720 - 740 nm) yielded the best performance for biomass. Another conclusion was that SRIs always performed better than NDVIs, but the combination ranges evidenced by the two indices were the same.

Another study analysing vegetation biomass in river floodplains using imaging spectroscopy showed that regression models with VIs and field measurements could be improved when differences in vegetation structure were taken into account (Kooistra et al., 2006). Better regression models have been achieved for individual plant functional types (grassland, shrub, mixed herbaceous and softwood forest).

To conclude, there have been numerous attempts to model biomass with hyperspectral data by using vegetation indices, but to our knowledge, no study exist that uses this technique for biomass modelling of alpine grassland.

2.3 APEX

The Airborne Prism Experiment (APEX) is an airborne imaging spectrometer developed under the scientific lead of a Swiss-Belgian collaboration between the Remote Sensing Laboratories (RSL, University of Zurich (CH)) and the Flemish Institute for Technological Research VITO (B) on behalf of the European Space Agency (ESA) PRODEX programme. The industrial consortium is headed by RUAG Aerospace (CH) with subcontractors such as OIP Sensor Systems (B) and Netcetera AG (CH). Special contracts were issued by ESA

for the development of a shortwave-infrared detector (Sofradir, (F)), and a calibration facility at the German Aerospace Center (DLR). The sensor is intended as a simulator and a calibration and validation device for future spaceborne hyperspectral imagers (Itten et al., 2008) The development started in 1993, and from 2008 - 2010 the sensor was in the calibration and testing phase. APEX was formally accepted by ESA at the end of 2010 and the sensors can be used commercially nowadays. Consequently, 2011 was the first year of commercial operations, resulting in two flight windows of a total of 7 weeks (Stessens, 2012).

APEX is built as a pushbroom dispersive imaging spectrometer recording more than 330 spectral bands contiguously. The instrument specifications can be found in Table 1. The APEX mission for the SNP acquired 186 km^2 at a 2x2 m spatial resolution determined by the sensor's instantaneous field of view (IFOV) in combination with a flight height of 4400 - 5400 m asl. 1000 pixels were recorded across-track with a data rate of 0.42 GBytes/km per flight path. The spectral configuration was set to 312 spectral bands to be acquired simultaneously. We used 301 bands for analysis, after some bands had to be removed due to noise. The sensor was installed on a Research Aircraft Dornier DO-228 aircraft (see Figure 5).

Table 1: Instrument specifications (from http://apex-esa.org, last accessed 20.12.2012)

Spectral Range	VNIR: 380 - 970 nm SWIR: 940 - 2500 nm
Spectral Sampling Interval	VNIR: 0.55 - 8 nm over spectral range (unbinned) SWIR: 5 - 10 nm over spectral range
Spectral Resolution (FWHM)	VNIR: 0.6 - 6.3 nm over spectral range (unbinned) SWIR: 6.2 - 11 nm over spectral range
Spectral Bands	VNIR: default 114 bands, reprogrammable through customized binning pattern SWIR 199 bands
Spatial Pixels	1000
FOV (across track)	28°
IFOV	0.48 mrad
Spatial Sampling Interval (across track)	1.75 m @ 3500 m AGL (2 - 5 m at flight altitudes of 4 - 10 km)
Sensor dynamic range	VNIR: CCD, 14 bit encoding SWIR CMOS, 13 bit encoding
Pixel size	VNIR: 22.5 µm x 22.5 µm SWIR: 30 µm x 30 µm
Smile (average over FOV)	0.35 pixels

Keystone (frown, average over FOV)	0.35 pixels
Co-Registration (average over FOV)	0.6 pixels
Signal-to-Noise	SNR for various applications are available upon request Highest signal to noise ratio through advanced detector technology and pressure / temperature stabilization

Figure 5: Picture of the Dornier DO-228 on which the sensor was installed, and the APEX sensor (Images from RSL, University of Zurich)

The instrument consists of a collimator that directs the light transmitted by the slit towards the prism, where a dichroic beam splitter separates it over two sensors: one sensitive in the VNIR and one sensitive in the SWIR wavelength range (Schaepman et al., 2003). The sensor is temperature and pressure stabilized and equipped with a built in “In-Flight” calibration facility. A control and storage unit (CSU) is available for the flight management to save navigation via GPS as well as the recorded data.

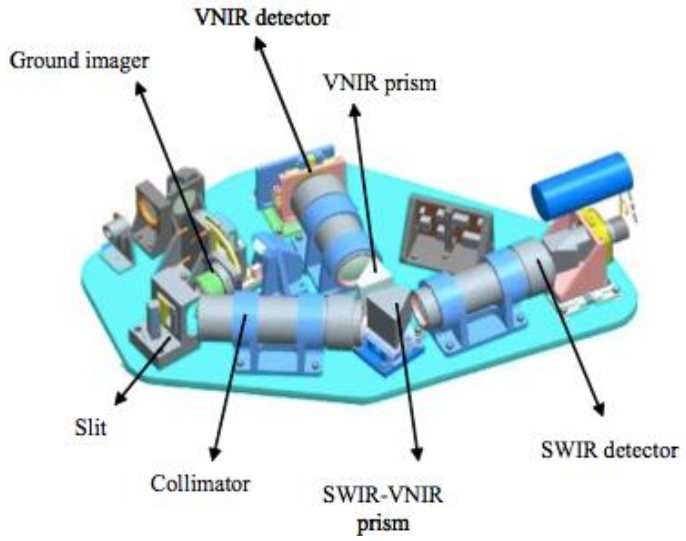

Figure 6: Overview of APEX subsystems (image from Schaepman et al., 2003).

The external facilities are the Calibration Home Base (CHB) for instrument calibration, which is located at the DLR in Germany, and a data processing and archiving facility (PAF) for operational product generation, which is managed by VITO (Jehle et al., 2010).

3 METHODOLOGY

The high spectral and spatial resolution of APEX data allows the correlation of the measured reflection with ground truth data. The generation of the biomass prediction map of the grassland of Val Trupchun is carried out by a statistical model which is optimized by the best calibration result.

3.1 THE STUDY AREA

The study site is located in the upper Engadin valley in south-eastern Switzerland (46°40'N, 10°15'E), within the territory of the Municipality of S-chanf. Val Trupchun was integrated into the national park in three steps, shown in Figure 7. The left (north) side of the valley has belonged to the park since its foundation in 1911, while the innermost part of the valley including Alp Trupchun followed in 1932. The right (south) side of the valley was joined in 1961.

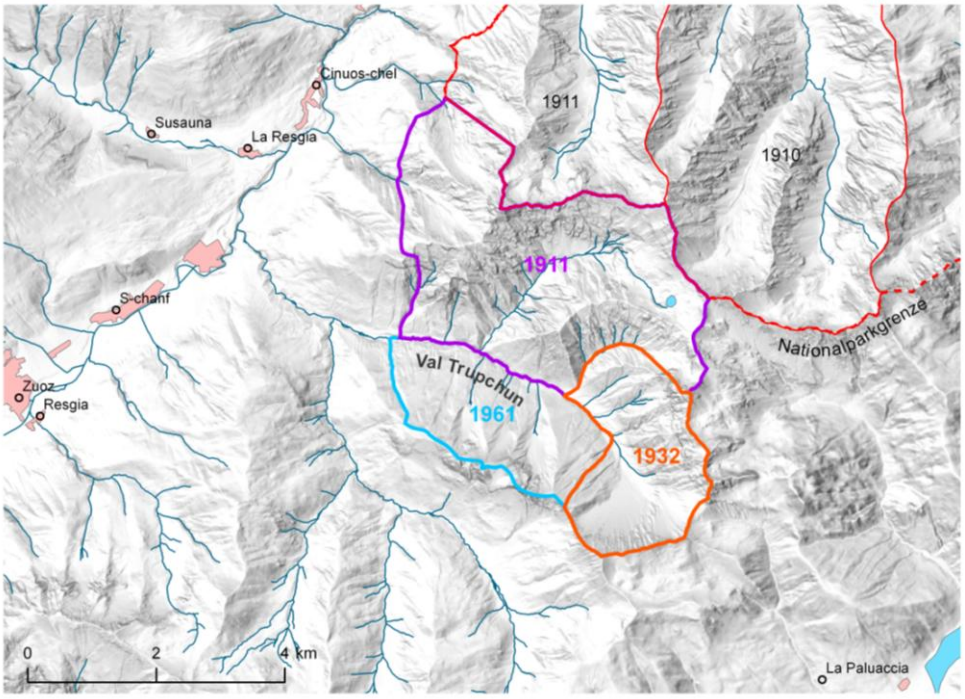

Figure 7: Overview of the study site Val Trupchun and its historical park boarders

The area is famous for its exceptionally high densities of ungulates: alpine ibex *(Capra ibex,* L.*)*, chamois *(Rupicapra rupicapra,* L.*)* and red deer *(Cervus elaphus,* L.*)*. The valley covers an area of about 23 km^2 and is dominated by grassland communities distributed over a large altitudinal range (1800 - 2600 m asl.) which represent the forage resources for ungulates. Forest, rocks and snow are the other land cover types to be found. The valley extends from east to west with very steep slopes of up to 78°. The bedrock is mainly composed of limestone and calcareous schist. The climate of the area is alpine. Average annual precipitation is ca. 700 mm with precipitation maxima in summer (June to August, 275 mm) and minima during the winter months (November to April ca. 215 mm), when precipitation consists of snow. The growing season starts late, especially at higher altitudes and on the north side of the valley, so that the different phenological stages occur simultaneously. The forest, which mainly consists of mountain pines (*Pinus mugo,* Turra), larches (*Larix decidua,* Mill.) and some Swiss stone pines (*Pinus cembra,* L.), reaches an altitude up to about 2150 m asl., followed by grassland at higher altitudes. Above the slopes, the land cover consists only of rock, covered by year-round snow at some locations. The former alp, which originates from the land use before the park foundation, is located at the end of the valley at 2040 m asl., where the old alp hut still exists.

3.2 FIELD DATA COLLECTION

Fieldwork was carried out to collect ground-truth data of the grassland. Twenty-five plots had previously been defined, which were distributed over the valley and at various altitudinal gradients in order to account for differences in species composition, productivity, phenological stages and soil type. A map with the sample plots indicated is shown in Figure 8.

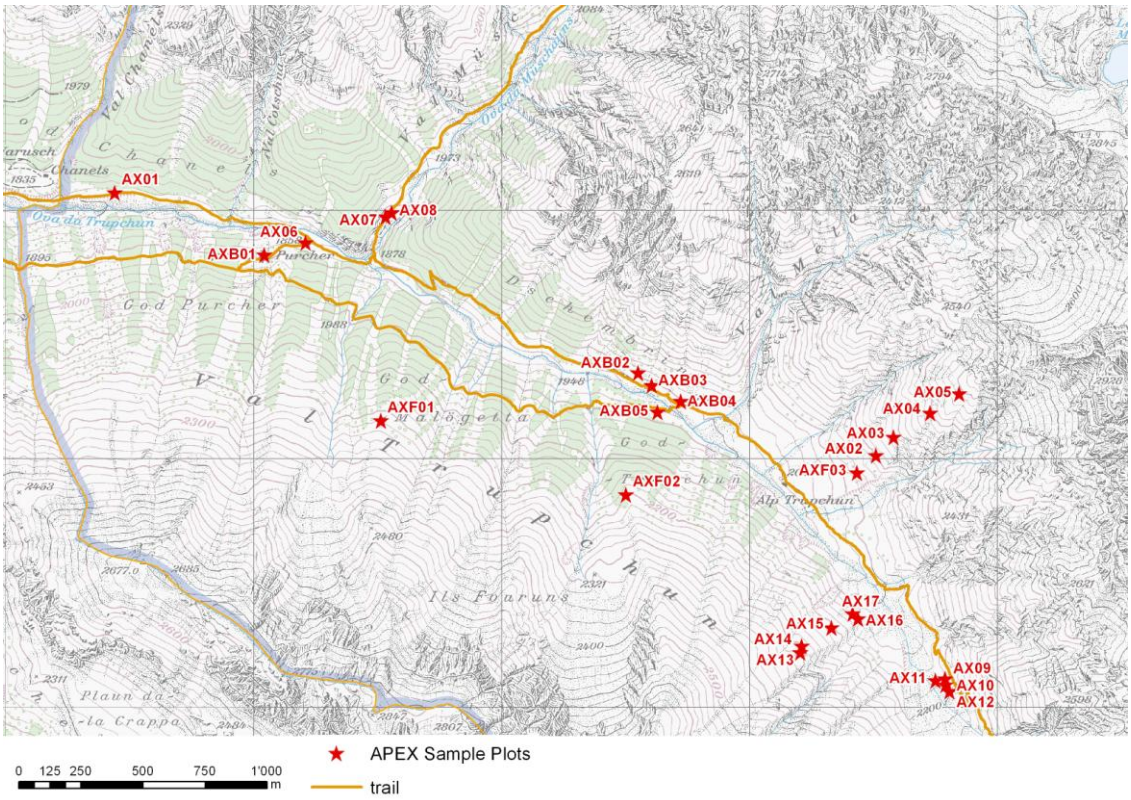

Figure 8: Locations of the 25 sample plots in Val Trupchun, where 1x1 m of vegetation was clipped.

The first plot is located a short distance behind the park entrance in a large forest clearance (AX01). Two plots are located at the Alp Purcher (1860 m asl.), an old alp from the time before the park (AX06 and AXB01). AX07 and AX08 are situated at the entrance of Val Müschauns, a side valley of Val Trupchun. AXB02, AXB03, AXB04 and AXB05 are located further back in the valley near a picnic area close to the trail, AXB02 and AXB03 on the Dschembrina side and AXB04 and AXB05 close to the bridge. AXF03, AX02, AX03, AX04 and AX05 are the plots at the northern slope of the valley covering an altitudinal gradient of 500 m up to 2500 m asl. at the top. Opposite are the plots AX17, AX16, AX15, AX14 and AX13 along the southern gradient, reaching an altitude of 2310 m asl. AX09, AX10, AX11 and AX12 are plots at the very end of the valley, at about 2200 m asl. and enclosed by steep slopes. AXF01 and AXF02 are two plots at the southern slope at God Malögetta and God Trupchun (both 2200 m asl.). More detailed maps of the plots can be found in Appendix A.

The plots were chosen at locations with vegetation as homogenous as possible, and squares of 6 x 6 m were marked. The corners of the plots were marked with flags and

measured with a differential global positioning system (GPS), device type Leica RX 1210 T. On 24 of June 2010, on the same day as the flight, above-ground biomass was clipped within a $1m^2$ subplot located in the middle of each plot (see Figure 9). The vegetation samples were sealed in plastic bags and weighed the same day in order to determine wet biomass. Afterwards, the samples were dried in the oven at 65° for 48 hours and weighed again to determine dry biomass.

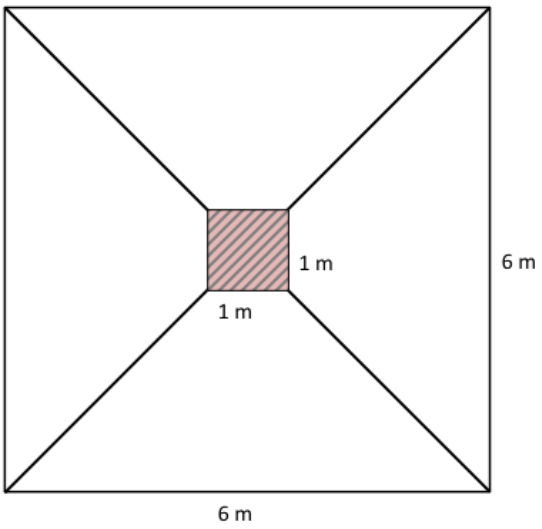

Figure 9: Apex ground truth plot design 2010

3.3 IMAGE ACQUISITION AND PRE-PROCESSING

The APEX flight was carried out on 24 of June under cloud free conditions. The acquired image data covers the whole territory of the Swiss National Park. The images were collected at solar noon at an average flight height of 6500 m above sea level (asl.). The specific study site Val Trupchun was covered by four image strips, each with an extend of about 2x6 km and a ground resolution of 2 m. The flight lines are SW to NE oriented, cross-wise to the valley and the mountain ridge (see Figure 10). The sun position in terms of solar zenith (SZ) and solar azimuth (SA) for the image strips were about SZ=66.2° and SA=166.9°. The APEX sensor comprised 301 wavebands, operating over a wavelength range of 380 - 2500 nm with an average spectral resolution of 3.45 nm in the VNIR (380 - 970 nm) and 8.6 nm in the SWIR (940 - 2500 nm) (cf. chapter 2.3, Table 1).

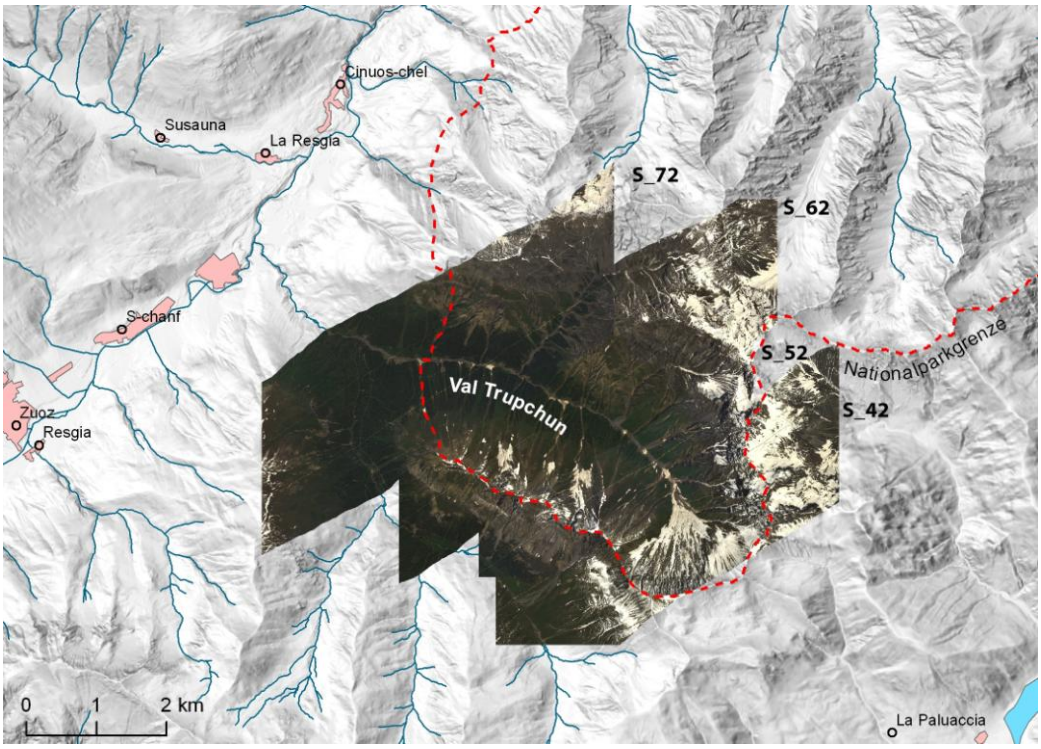

Figure 10: Overview of the study site and the 4 flight strips (S_42, S_52, S_62 and S_72)

The image strips were atmospherically and geometrically corrected by RSL using standard procedures. The atmospheric correction was computed using the ACTOR-4 software tool to obtain hemispherical-conical-reflectance (HCRF) data (Schläpfer & Richter 2002). The geometrical correction was made using the Parametric Geocorrection (PARGE) software (Schläpfer & Richter, 2002) and data were afterwards transformed in the Swiss coordinate system LV 03. The geo-corrected APEX data can be overlaid with other auxiliary data (e.g. a digital elevation model DHM25) and directly related to the biomass ground-truth data. The geometric distortions of the orthorectified data were evaluated based on ground based GPS measurements and were found to be less than one pixel (+/- 2m) (Damm et al., 2012). However, there were differences between the reflectance of similar pixels in the overlapping regions between image strips due to different view angles and effects of surface anisotropy (Weyermann et al., 2013).

3.4 DATA ANALYSIS

To extract APEX reflectance data at the sample locations, the following procedure was applied: A square of 6x6 m around the centre coordinate of the plots was imported

into the ENVI 4.7 software. This square corresponded to 9 pixels (3x3 pixels) of the APEX data from which the average reflectance was extracted as reference value. There were plots lying on more than one strip because of the overlapping zone, so that two reference reflectance values were available for one sample. These values were considered as independent measurement points. Consequently, there were 43 measurement points available, from which 18 points were double (same ground truth biomass value, but different reference reflectance).

The biomass samples were divided into two groups, one used for the calibration (22 points), and one for the validation (21 points) of the model using a stratified random sampling approach. An empirical model was developed based on the 22 calibration samples. The standard NDVI was calculated based on band 50 (664.3 nm) and band 86 (808.8 nm) by using the following formula:

$$NDVI = \frac{NIR - RED}{NIR + RED} = \frac{R_{808.8} - R_{664.3}}{R_{808.8} + R_{664.3}}$$

where *R* is the reflectance at the specific wavelength.

The calculated NDVI was regressed against the calibration biomass samples in an exponential regression to obtain the coefficient of determination (R^2) for calibration. An exponential (instead of linear) regression can be implemented due to the large volume scattering of vegetation that induces sensor saturation at high densities.

Since APEX provides more bands in the red (600 - 700 nm) and NIR (700 - 1300 nm), we tested if calibration results could be improved by calculating simple ratio vegetation indices (SRI) with all possible combinations of 301 bands and regressing them against the calibration data set.

$$SRI = \frac{R_a}{R_b}$$

where R_a and R_b is the reflectance at wavelength a and b, respectively.

Spearman's rank correlation coefficients (R) resulting from the regression analysis were plotted on a 2D-contour plot to evaluate R characteristic patterns and identify

the best wavelength combination. This procedure allowed the selection of optimal bands to be used in the calculation of the index. Band combinations with maximized correlation with biomass were chosen, considering cause effect relationships between spectral bands and underlying absorption and scattering processes. For the final model we chose the best SRI within the range of the visible (RED) for the first band and near-infrared (NIR) (700 - 1300 nm) region for the second band. Within this range, high reflection occurs on healthy biomass, and no water absorption interferes with the signal. With the chosen SRI we computed an exponential regression model to predict and map biomass content.

Predictive performance of the biomass model was computed with the independent validation data set. The coefficient of determination (R^2) and the root mean square error (RMSE) were calculated to compare the predicted with the observed values.

Secondly, a SRI model was calculated with another band selection to test the problem of underestimation in the region of high biomass, usually occurring with NDVI and SRI models with a broad band selection. Two narrow bands in the far RED were chosen as this should solve the saturation problem according to Mutanga and Skidmore (2004).

Furthermore an investigation about the APEX data regarding the overlapping zone between two strips was carried out. As SRI values on overlapping regions vary slightly between the strips, the different SRI from plots located on more than one strip are analysed in a scatterplot.

Then an analysis about the variability of the APEX pixel location is conducted. The average SRI at the sample plot locations were extracted for the 5x5 pixels around the centre coordinate and compared to the result of 3x3 pixels. This value was converted by the SRI biomass model equation to analyse the difference with respect to the biomass prediction. The biomass discrepancy predicted for the sample plot locations are compared and discussed in a histogram.

The biomass prediction model is only valid for grassland. A linear spectral unmixing method (LSU) was performed to separate different land cover classes and to extract

the grassland. LSU is a classification approach that can be used for hyperspectral imagery based on the materials' spectral characteristics. The reflectance at each pixel of the image is assumed to be a linear combination of the reflectance of each material present within the pixel (Boardman, 1989). The measured spectrum of a mixed pixel is decomposed into the set of corresponding fractions (endmembers) that indicate the proportion of each endmember present in the pixel. Pure training pixels were manually defined for grassland, rock, snow and forest in selecting homogenous pixels as regions of interest. The linear unmixing method is then assigning each pixel into the predefined classes based on the abundance values of each endmember. The unmixing result has a data range (representing endmember abundance) from 0 - 1. 50% has been taken as abundance for extracting grassland.

4 RESULTS

For the calibration data set, 22 sample plots were randomly chosen out of 43 independent reflection reference values from all sample plots. The plots lying in overlapping regions of two strips were taken as independent reflection references, as different reflectance values were available. A table with the specific calibration and validation points of all sample plots can be found in Appendix. For all correlations between biomass sample and APEX reflectance spectra, the comparison was carried out using the wet weight of the biomass samples. The wet weight achieved overall better R^2 compared to the dry weight.

4.1 FIELD SAMPLE RESULTS

In Table 2 the results of the field campaign can be found. The dry and the wet weight of all 25 biomass samples are listed. The samples were overall in a reasonable range with a mean average of 400 g/m^2 (SD = 80 g/m^2) for the wet weight and 126 g/m^2 for the dry weight (SD = 260 g/m^2). The minimum was found at Alp Trupchun East (37 g/m^2). High biomass was found especially on former alp sites, at Alp Purcher (AX06), Alp Trupchun (AX14) and at the entrance of Val Müschauns (AX07).

Table 2: Overview of the raw data of all biomass samples

Plot	*Height* m asl.	*Dry weight* [g/m^2]	*Wet weight* [g/m^2]	*Location*
AX11	2174	9.31	37.2	Alp Trupchun E
AX16	2141	36.91	78.3	Alp Trupchun S ++
AX12	2202	16.62	90.9	Alp Trupchun E
AX10	2193	28.03	135.1	Alp Trupchun E
AX04	2406	61.96	181.5	Alp Trupchun N +++
AXF03	2141	89.39	230	Alp Trupchun Falle N
AX05	2491	96.72	181.6	Alp Trupchun N ++++
AXF02	2209	49.74	207.1	God Trupchun S oben
AXB02	2014	123.55	352.8	Dschembrina W
AX09	2190	66.38	288.8	Alp Trupchun E
AX13	2313	82.9	250.7	Alp Trupchun S +++++
AX08	1898	103.16	442.1	Val Müschauns E
AXB03	1998	152.84	414.5	Dschembrina E
AX02	2208	148.08	425.7	Alp Trupchun N +
AXB04	2004	149.69	385.4	Brücke N
AX03	2282	170.53	496.8	Alp Trupchun N ++
AX17	2135	192.92	464.6	Alp Trupchun S +
AXB01	1893	97.76	424.5	Purcher S oben
AXF01	2222	137.41	483.6	God Malögetta
AXB05	1985	102.74	487.5	God Trupchun S unten
AX01	1823	191.62	614.2	Trupchun Eingang Wiese
AX15	2204	175.33	552.6	Alp Trupchun S +++
AX14	2297	327.4	683.1	Alp Trupchun S ++++
AX07	1896	248.59	858.9	Val Müschauns W
AX06	1861	285.36	1235.4	Alp Purcher
Mean	2127	126 (SD=80)	400 (SD=260)	

4.2 REGRESSION OF BIOMASS AND STANDARD NDVI

The standard NDVI was calculated using APEX band 50 and 86 located at 664.3 nm and 808.8 nm. A correlation with the calibration data set was computed, and an exponential regression yielded the best fit with an R^2 of 0.74, shown in Figure 11.

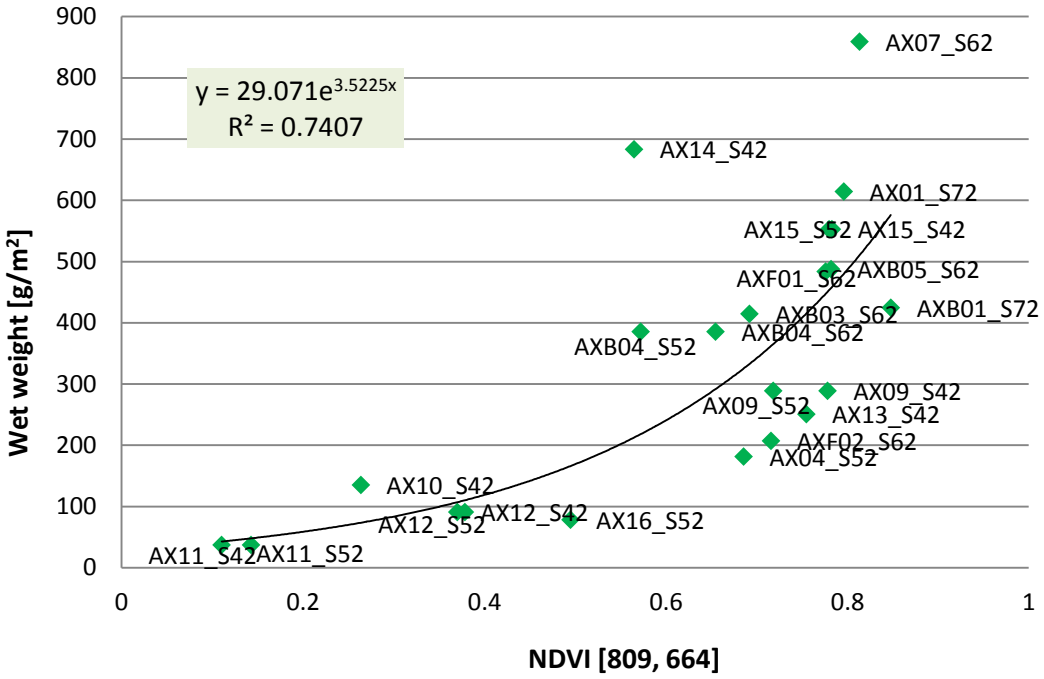

Figure 11: Regression between the standard NDVI derived from APEX reflectance spectra from bands at 809 and 664 nm and the wet weight biomass calibration sample data

The validation of the model was carried out by calculating the predicted biomass using the calibration model at the validation sample plots and comparing them against the true wet weight values. The R^2 and the RMSE were 0.54 and 236 g/m^2 respectively, shown in Figure 12.

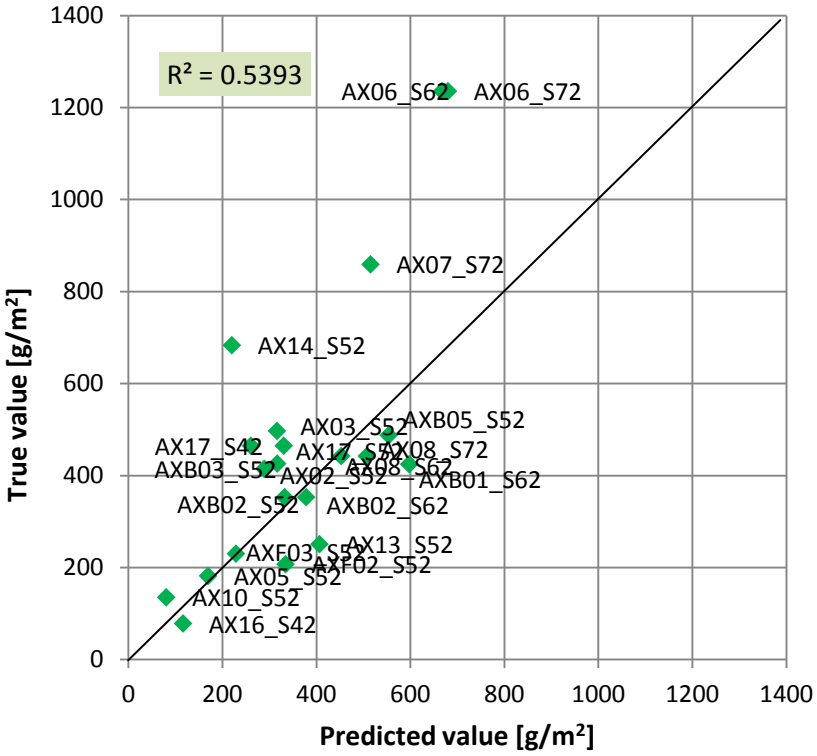

Figure 12: Regression between the predicted biomass value calculated from the NDVI model calibration and the true biomass value of the validation sample plots

Plots AX06, AX07 and AX14 are located furthest from the 1:1 line. AX06 is located at Alp Purcher, next to a former alp hut, where tall-herb communities dominated by stinging nettle (*Urtica dioica*, L.) and monkshood (*Aconitum napellus ssp. Vulgare,* DC.) occur. The model predicts that there should be less biomass than the measured value. The biomass at AX14 is also underestimated from the model. The second value of this plot from strip S42 already deviates from the calibration curve. This plot is situated on the southern gradient at 2300 m asl. AX07 is situated at the entrance of Val Müschauns on a spot with ruderal vegetation.

It can be concluded that the model based on the standard NDVI generally underestimates biomass values above 600 g/m^2.

4.3 Regression of Biomass and Optimal Simple Ratio Index

To optimize the model, simple ratio indices (SRI) were calculated with all possible combinations of bands and correlated against the calibration data set. Spearman's

rank correlation coefficients (R) were plotted on a 2D-contour plot to identify the best wavelength combination, shown in Figure 13.

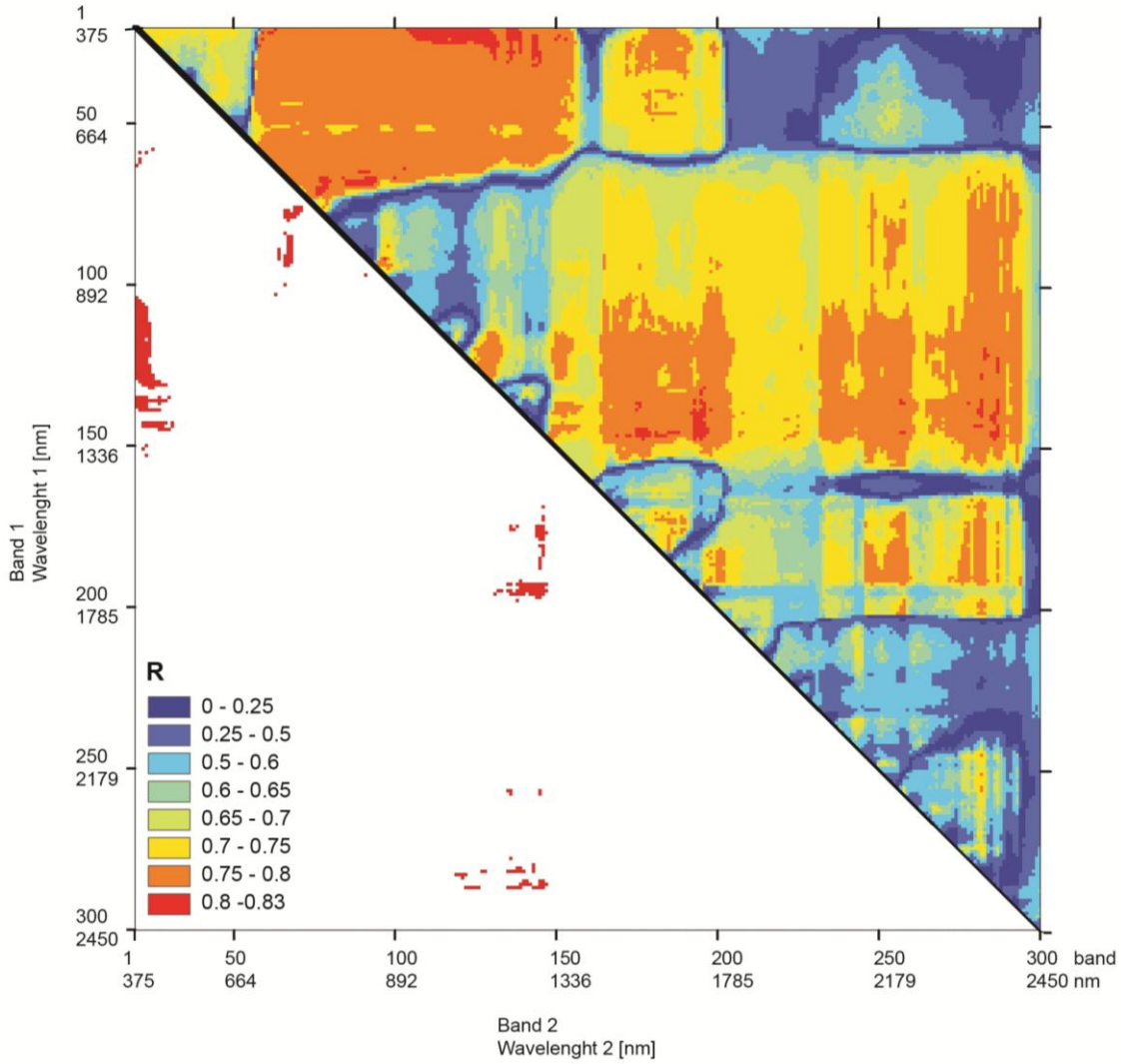

Figure 13: 2D-correlation plot that shows the correlation coefficient R (Spearman's Rank) between SR indices and biomass. The matrix is symmetrical. Below the diagonal, band combinations are marked in red where R>0.8.

High correlations were found between one band in GREEN and one band in NIR, one band in RED and one in NIR with overall highest R = 0.823, and one band in NIR and one in SWIR-1. A table with band combinations R > 0.8 can be found in Appendix B.

For our final biomass model the best SRI within the range of visible (RED) and near-infrared (NIR) (700 - 1300 nm) region was chosen. Within this range high reflection on healthy biomass occurred and no water absorption interfered with the signal. Another argument was to choose a band close to the diagonal 1:1 line. The closer the two

bands are, the smaller are the atmospheric and external influences. This can be observed by comparing the SRI values at the plot locations that lie on two strips. The differences between SRI of the two strips are lower with band combinations closer together.

The SRI of band 92 (842 nm) and band 68 (727 nm) achieved the best R (0.823) overall and fulfilled the selection criteria. Figure 14 illustrates the spectrum of a typical grassland pixel from our site with the two chosen bands indicated.

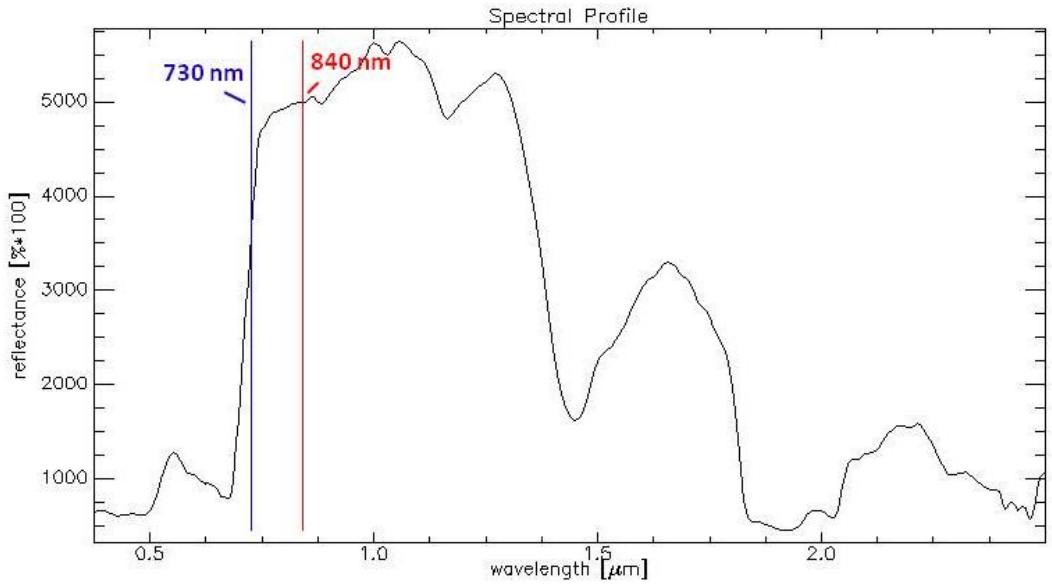

Figure 14: Reflectance spectra of a typical pixel of the grassland in Val Trupchun. The blue mark indicates the band at 730 nm and the red mark the band at 840 nm

This combination was chosen for the final biomass model. An exponential regression model was computed again between SRI and wet weight biomass of the calibration data set resulting in an R^2 of 0.77 (Figure 15).

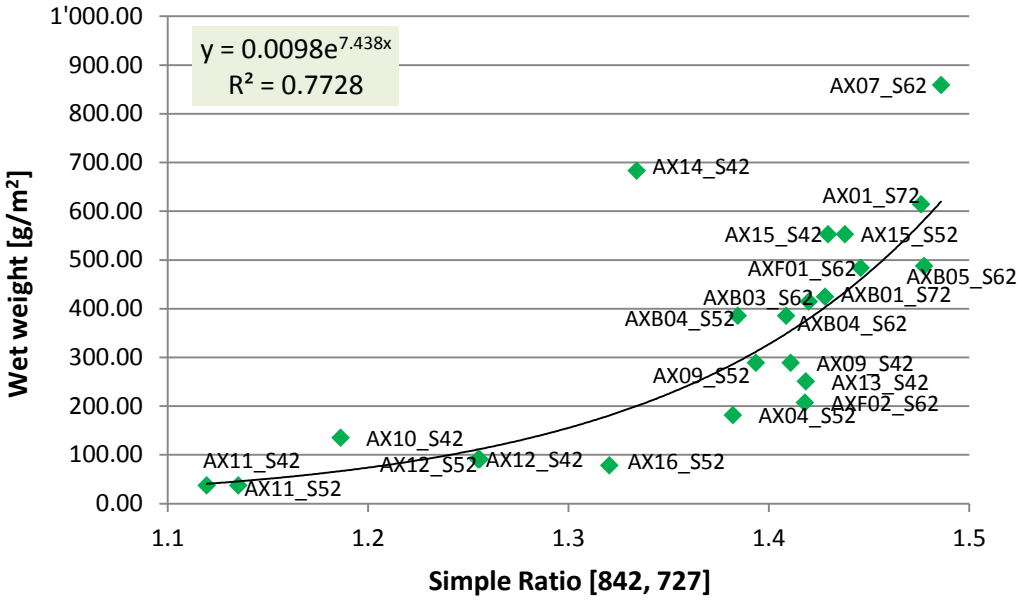

Figure 15: Regression between SRI derived from APEX reflectance spectra from band at 842 nm and 727 nm and the wet weight biomass calibration sample data.

The validation of the model was carried out by calculating the predicted biomass using the model equation for the validation sample plots and comparing them to the true wet weight values. The R^2 and RMSE were 0.57 and 238 g/m^2 respectively, shown in Figure 16.

Generally the pattern of the plots was comparable to the NDVI model. The outliers were again AX14, AX06 and AX07. The calibration model under-estimated biomass values above 600 g/m^2.

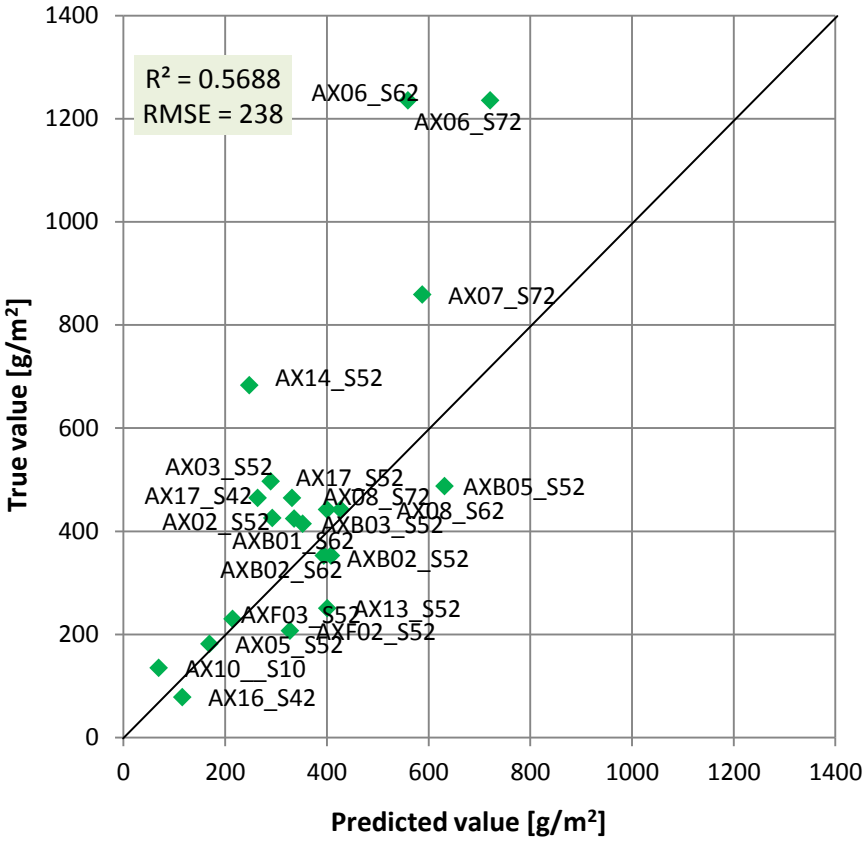

Figure 16: Regression between the predicted biomass value calculated from the SRI model calibration and the true biomass value of the validation sample plots

4.4 REGRESSION OF BIOMASS AND NARROWBAND SRI

According to Mutanga and Skidmore (2004) a narrow band SRI, both located in the far RED (around 750 nm) should solve the saturation problem which means that sample locations with high biomass occurrence aren't underestimated.

To analyse this thesis, the best R around two bands in the far RED was selected from the 2D-correlation plot (cf. Figure 13). The SRI between band 77 at 765 nm and band 70 at 735 nm has an R of 0.810 and is thus only slightly lower compared to the highest R (0.823) for the optimal SRI at bands 92 and 68. The model was recalculated with these two bands to check for a possible model improvement.

The exponential regression is shown in Figure 17. The coefficient of determination (R^2) is 0.7697, which is only slightly lower than our best SRI (R^2 = 0.7728). On the other hand, the validation shown in Figure 18 yielded 10% better validity (67%). High

biomass values were still underestimated (AX06, AX07, AX14), but at a lower level than with the best SRI model.

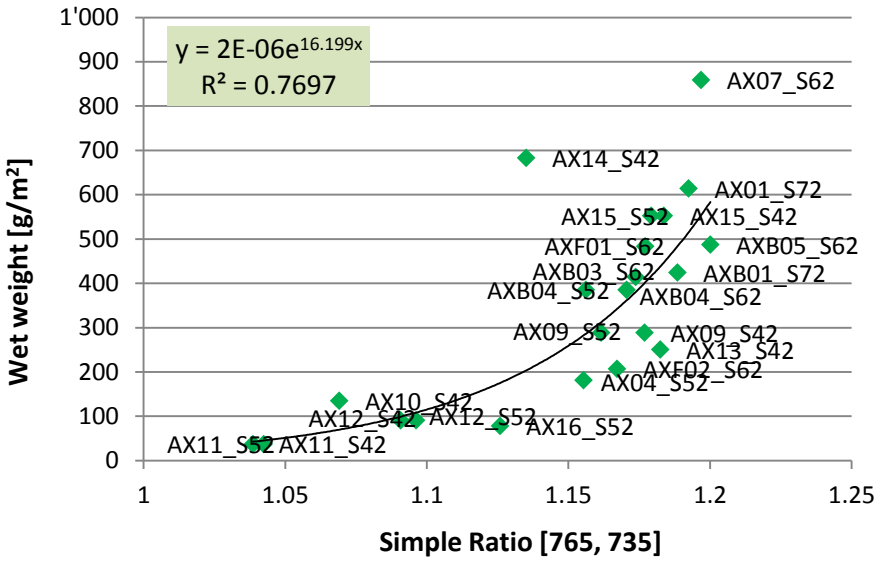

Figure 17: Regression between SRI derived from APEX reflectance spectra from band at 765 nm and 735 nm and the wet weight biomass calibration sample data

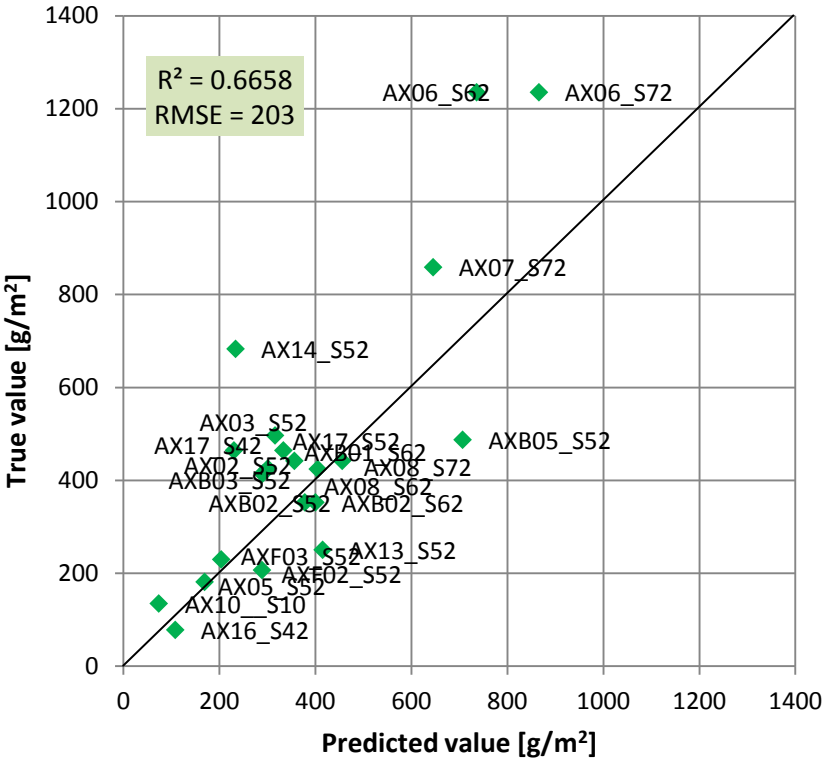

Figure 18: Regression between the predicted biomass value and the true biomass value for the prediction model $SRI_{765\ nm,\ 735\ nm}$

4.5 BIOMASS MAP

The best SRI regression model (band 842 and 727 nm) that was found for the estimation of biomass was applied to the APEX image. Only image pixels representing grassland were considered. The grassland was extracted by carrying out an LSU classification with the APEX data. Figure 19 shows the resulting biomass prediction map.

Estimated biomass values were generally in a reasonable range. Biomass values were categorized into 10 classes for cartographic reasons. The class intervals were computed by steps of ½ standard deviation. On the map, it can be seen that biomass decreases with increasing altitude at the slopes. Three locations with high biomass are noticeable. The highest biomass sources are located around the former Alp Trupchun. High sources are also visible around former Alp Purcher. Another spot with remarkably high occurrence is situated at the end of the valley on the bottom south slope.

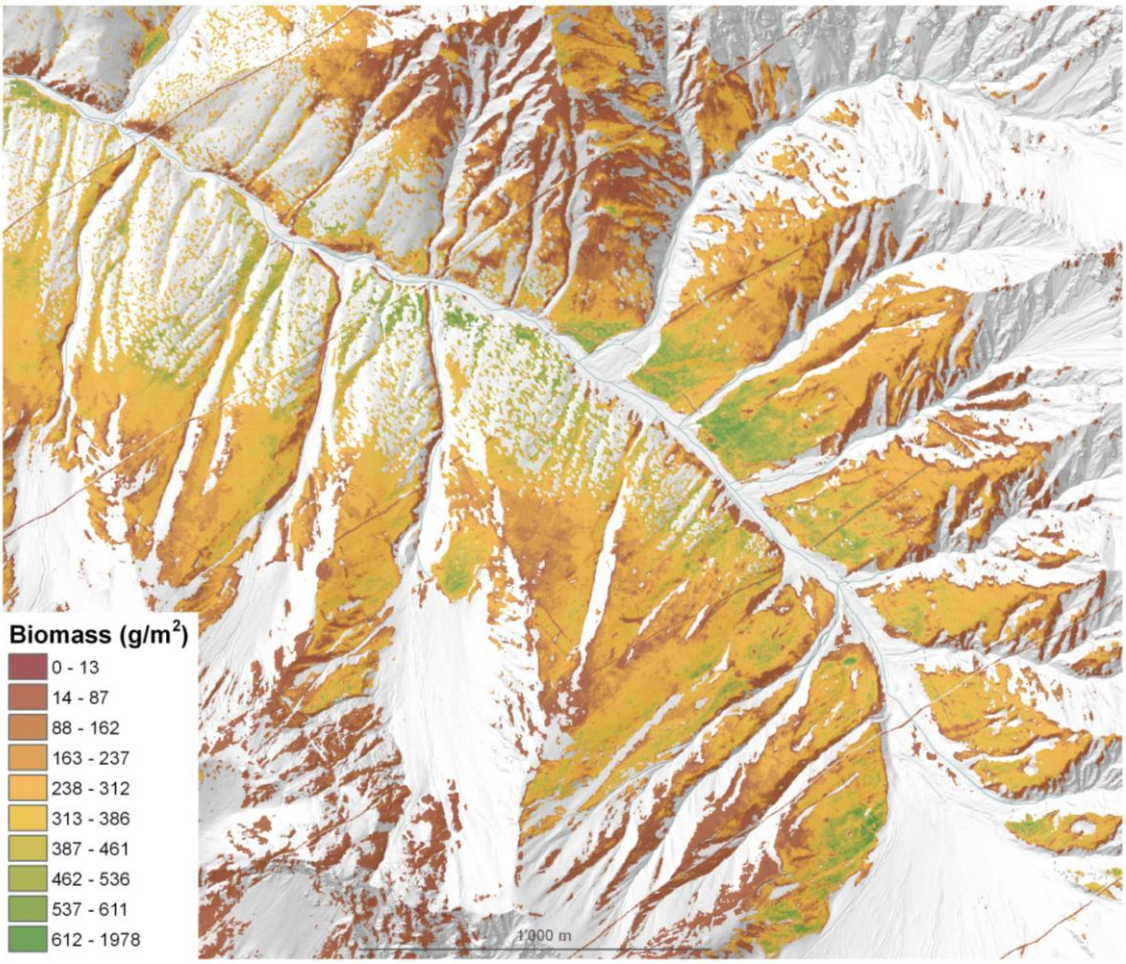

Figure 19: Biomass map of Val Trupchun overlain on a graphical relief shading

Figure 20 shows a close-up of the map around Alp Trupchun. To analyse the biomass source, the HABITALP dataset is overlaid. This map includes herb/grass functional types or dominant species if one vegetation unit stands out. It can be seen that high biomass correlates with the occurrence of monkshood. This means that excessive nutrients are available in this area which stem from former anthropogenic activities on the alp (cattle or sheep excreta). The alp hut can also be seen on the map. It's the small square with zero biomass, as well as the trail, where no vegetation grows.

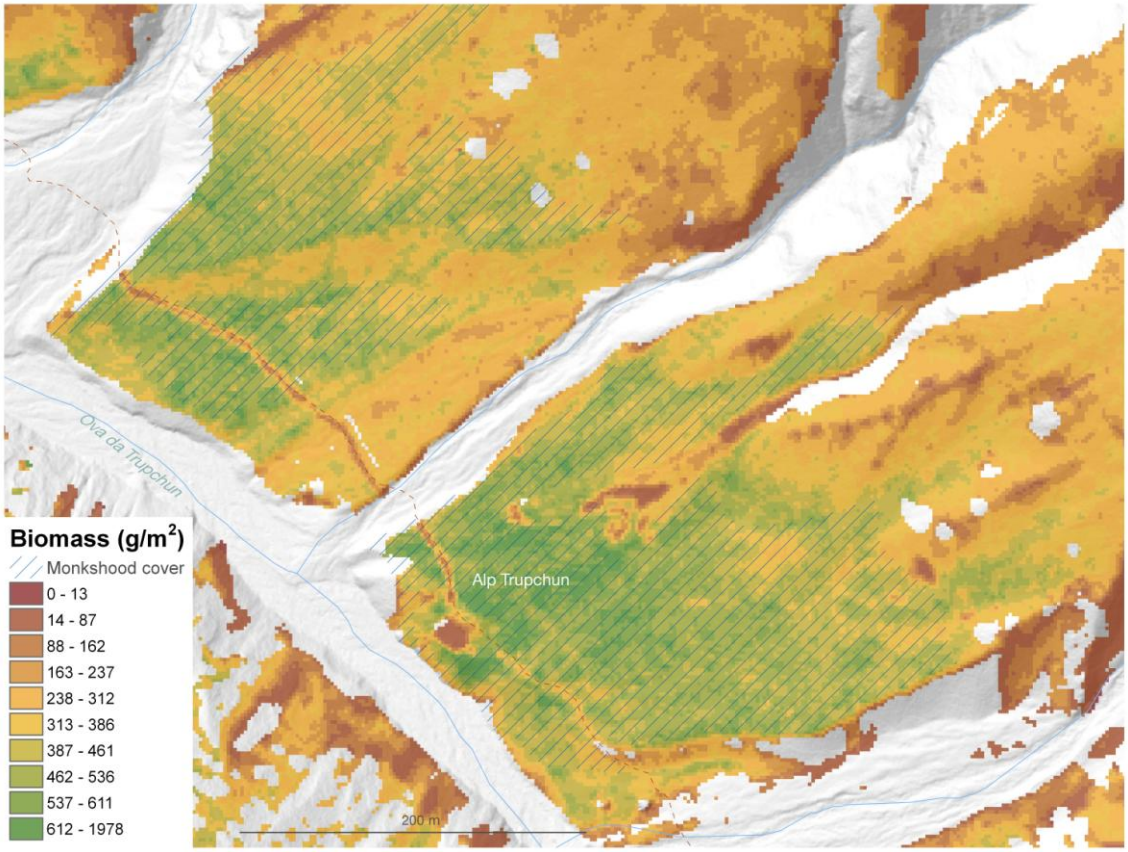

Figure 20: Detailed biomass map and monkshood occurrence of the grassland around Alp Trupchun

A detailed map of the area around Alp Purcher can be seen in Figure 21. There is a high biomass concentration around the old alp hut, where the trail diverts, and also on the right side of the entrance to Val Müschauns. A comparison with the grass/herb classification of the Habitalp map shows here that there is dominant stinging nettle coverage around Alp Purcher, which we also noticed during fieldwork. The right part of the pasture around the hut is characterised by dominant tall-herb communities, Megaphorbiae. The pasture in Val Müschauns is covered by ruderal vegetation. This spot next to the riverbed has low substrate and is mainly covered by tufted hairgrass (*Deschampisa cespitosa* L.), which is a densely tufted plant with a lot of biomass and little water content.

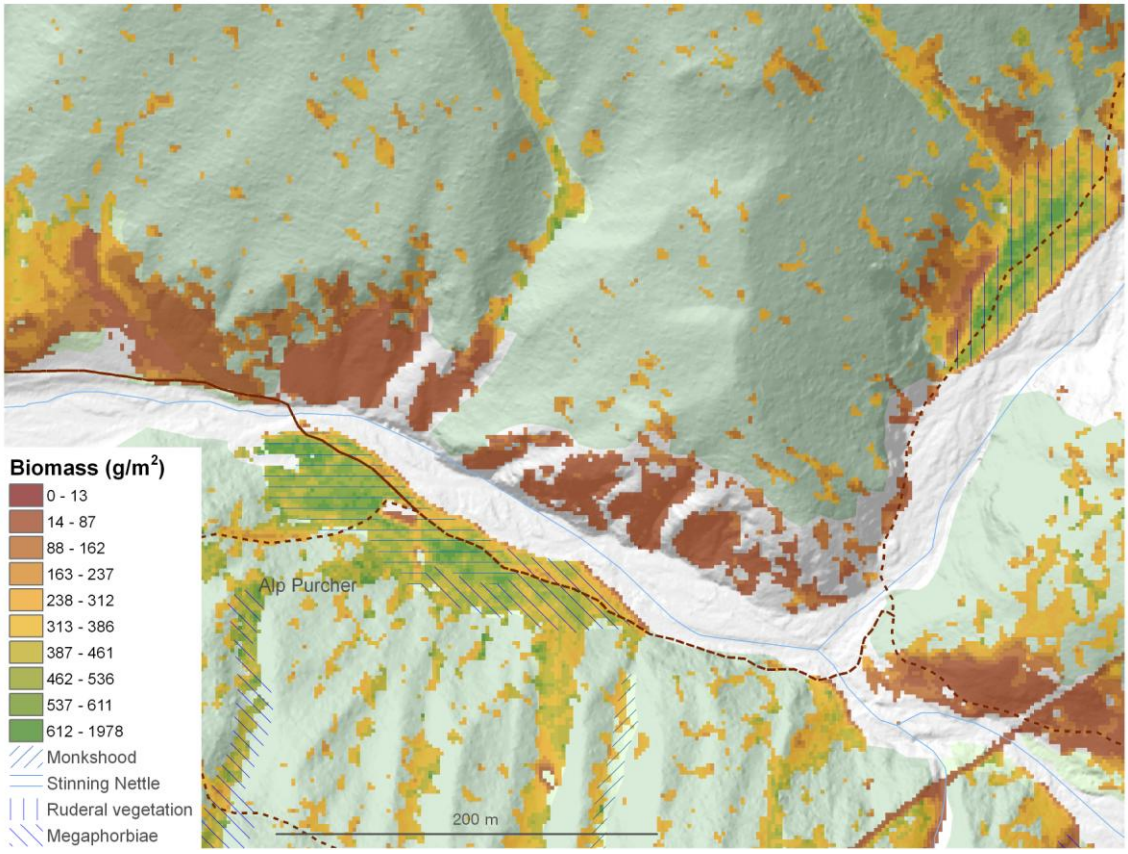

Figure 21: Detail map of Alp Purcher with special herb/grass type

The third spot with remarkable biomass occurrence situated at the end of the valley can be seen in Figure 22. The Habitalp map doesn't indicate a special herb / grass cover at this spot. The remarkably high sources must derive from good exposition, soil and moisture characteristics. However, it can be noted that on this site grazing and resting ungulates, mainly red deer, can be observed frequently, especially during summer months.

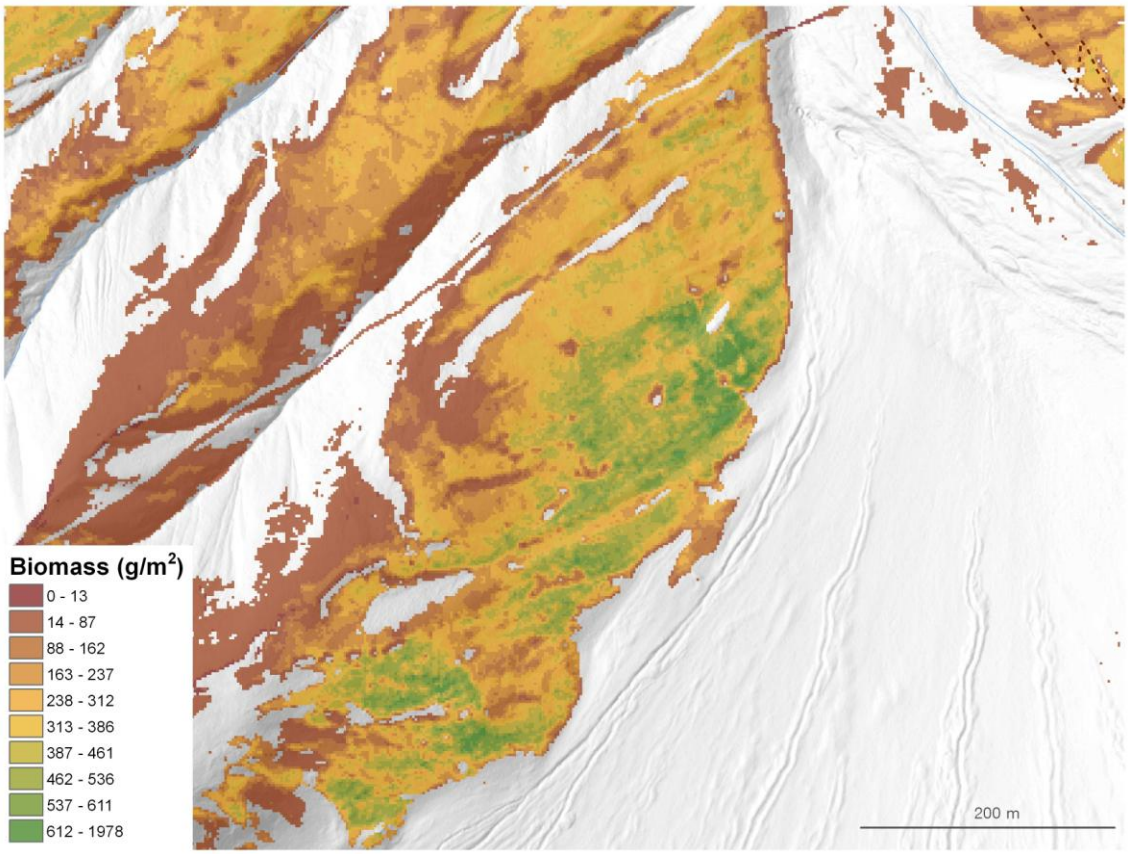

Figure 22: Detailed map of the bottom south slope in the back of the valley with high biomass sources

Figure 23 shows the histogram of the biomass map. Most values are in the range of 200 - 400 g/m^2. These are generally plausible values for alpine grassland. The average mean of all biomass samples on the territory of the SNP (standing crop) in 2010 was 355 g/m^2 in 2010 (SD=240 g/m^2) with a minimum of 20 g/m^2 and a maximum of 1235 g/m^2. These values didn't differ much in 2011 and 2012.

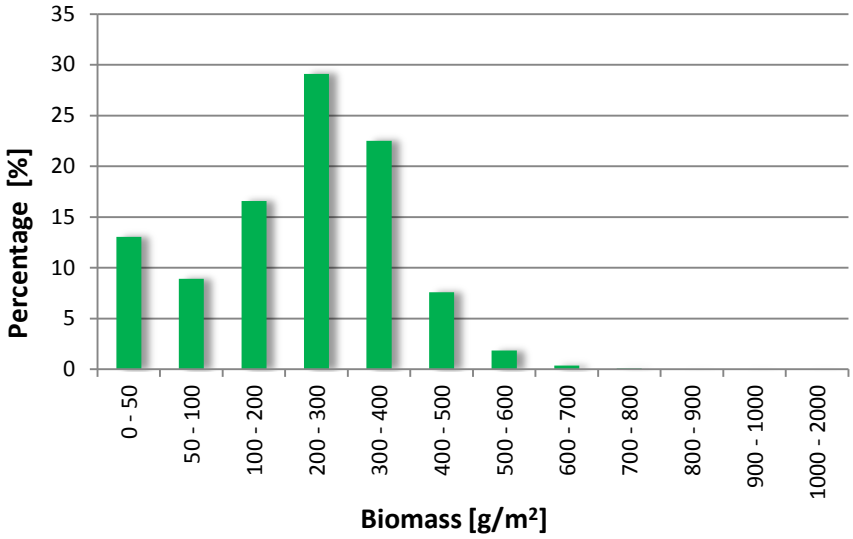

Figure 23: Histogram of the biomass map of Val Trupchun

4.6 DIFFERENT REFLECTANCE VALUES BETWEEN STRIPS

For the uncertainty analysis of our model an investigation of the sample plot location lying on more than one strip have been carried out. The differences of the SRI between the overlapping image strips were analysed by the variability of the plots located on two strips in a scatter plot (Figure 24). The analysis is first done for our optimal SRI with band 842 and 727 nm. The SRI value from one strip is plotted against the same SRI of the other strip for the double plots. The coefficient of determination R^2 is acceptable with 0.96. This factor is again dependent on the choice of band combinations because this effect is not constant over the bands. The same scatter-plot for the SRI with narrow bands (765, 735 nm) resulted in an R^2 of 0.95 (Figure 25).

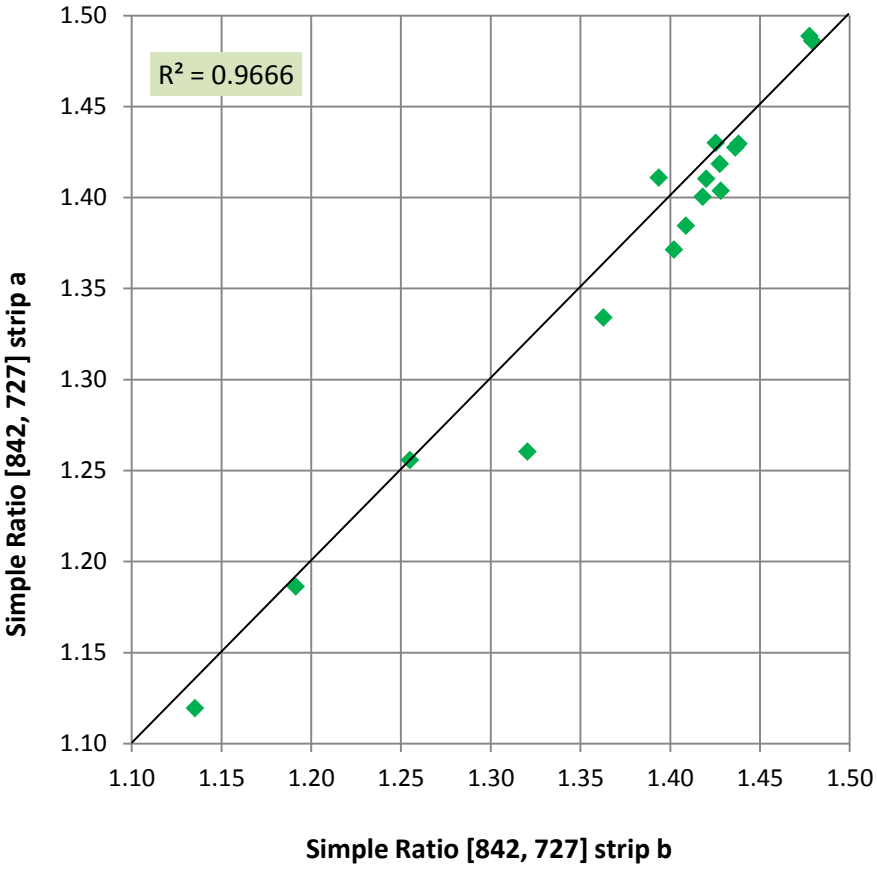

Figure 24: Scatter plot of the optimal SRI values of all sample plots on APEX strip a against strip b

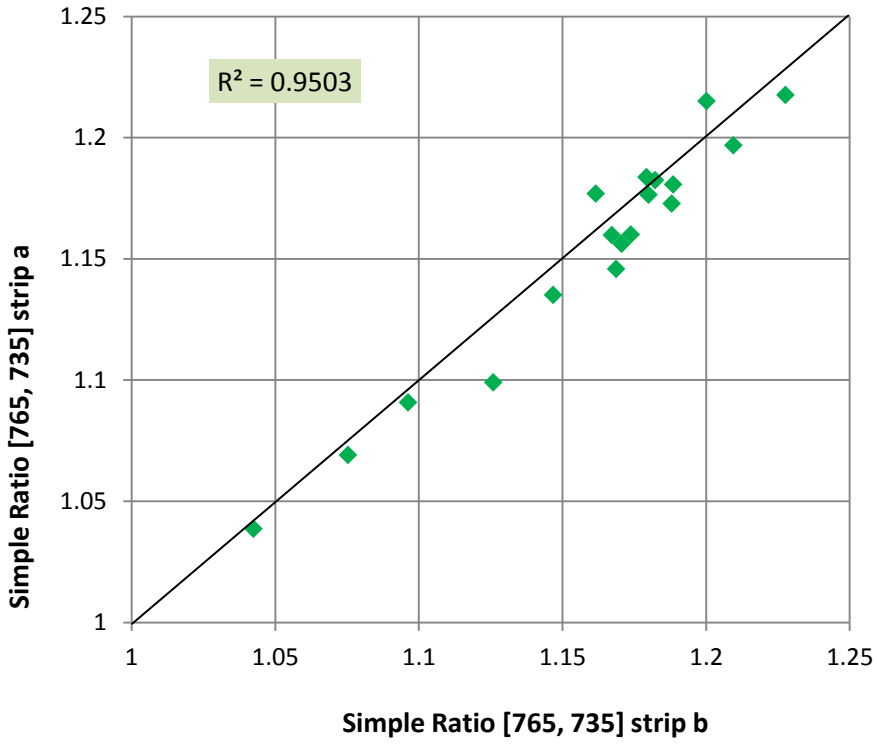

Figure 25: Scatter plot of the narrow band SRI values of all sample plots on APEX strip a against strip b

To quantify these differences with respect to the biomass prediction, the comparison was carried out implementing the modelled values. The result produced a mean error of 12% for the biomass on these plots.

Investigating the individual plots, the highest differences occurred at plot AX16 (32%), AX06 (22%), AX17 and AX14 (both ca. 20%). The results can be found in Table 5, Appendix B.

4.7 VARIABILITY OF SAMPLE PLOT LOCATION

Another analysis with respect to the uncertainty of our model was carried out by investigating the location of our sample plots. The correlation of the biomass sample data with the APEX pixel data was done by extracting the mean value of 3x3 pixels around the coordinate mid point of each plot. To analyse the impact of possible shifts, a comparison between average reflectance of 5x5 pixels (10x10 m) and 3x3 pixels (6x6 m) were carried out.

The average SRI from our optimal model with band 842 and 727 nm at the sample plot locations were extracted for the 5x5 pixels around the centre coordinate and compared to the result of 3x3 pixels. This value was converted by the biomass model equation to analyse the difference with regard to the biomass prediction. **Figure 26** shows the biomass discrepancy in percent for all sample plots, predicted with the new 5x5 pixels model and compared to the values of the 3x3 pixels model. A positive value on the y-axis means that the old model reaches a higher biomass prediction compared to the 5x5 pixels model and vice versa. The absolute mean difference is 4.6%, seen on the last bar.

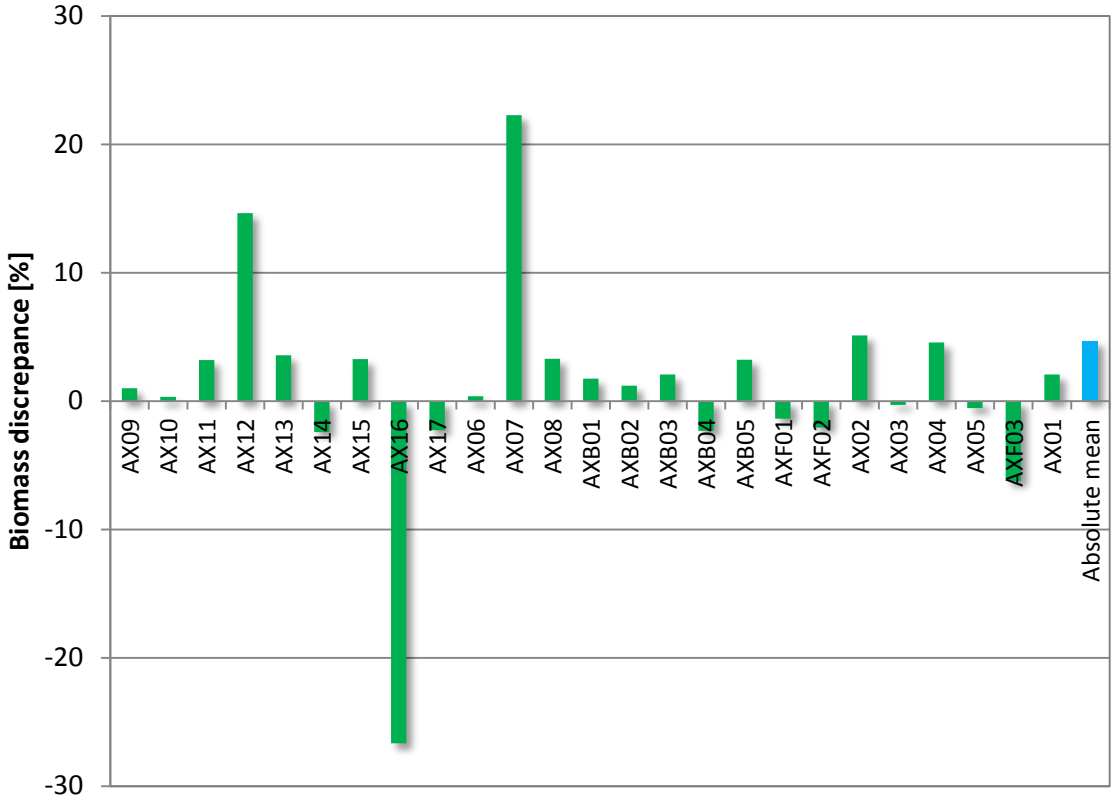

Figure 26: Biomass discrepancy predicted for the sample plot locations between implementation of average reflection of 3x3 vs. 5x5 APEX pixels as reference values.

5 DISCUSSION

In general high correlations with biomass ground truth were found. The optimized model was generated by implementing the best SRI. In the following discussion we found that the best calibration doesn't bring the best validation result. Many factors showed that the model validation vary strongly with different model input settings.

5.1 BIOMASS REFERENCE

The biomass field data was available as wet and dry weight. The regression analyses showed that wet weight correlated better with APEX data than dry weight. The reflection of the actual vegetation cover showed high volume scattering due to the water content and the leaf architecture. It makes more sense to correlate reflectance with wet weight because many different plant types are found within one plot and the water content of the different plants isn't constant.

We were not able to distinguish between dead and live biomass, i.e. between photosynthetically active (PV) and non-active vegetation (NPV). We tried not to sample the dead material, but as the grassland is very mixed and weedy, this was difficult to accomplish. At some plots there was only very little grass coverage (especially on the higher plots due to the late start of the growing season), so that all available material had to be cut.

5.2 COMPARISON OF NDVI AND OPTIMAL SRI

NDVI and SR indices are functionally related (Liang, 2005), however SR indices are often used in mountainous regions (Boschetti et al., 2007) since they enhance the contrast between soil and vegetation, minimize the effects of the illumination conditions (Baret and Guyot, 1991) and reduce shadow effects (Boschetti et al., 2007). Additionally, the presented results indicate a better performance of the optimal SRI compared to the NDVI and an improved the predictive accuracy of the SRI for biomass.

The coefficient of determination R^2 increased from 0.74 for the standard NDVI to 0.77 for the SRI model. The validation is also slightly improved from 0.54 to 0.56 (R^2). The quality of the model with an accuracy of 57% is good regarding the challenging terrain with slopes up to 78°. This means that 57% of the variation in biomass on an independent test data set could be explained by the model.

Both models are non-linear and underestimate high biomass values (above 600 g/m^2). Such bias can be caused by random noise or fundamentally non-linear relationship in the true physical relationship (Geladi et al., 1999). Another reason is saturation of NIR reflectance in dense vegetation, which frequently affects NDVI and slightly less SR indices. Broad bands for VIs, one in RED and one in NIR, have been shown to saturate at high biomass or high LAI (Mutanga & Skidmore, 2004). For our SRI we chose two closer bands (730 vs. 840 nm), still located in RED and NIR.

However, the saturation effect should only occur typically in multilayer vegetation such as forests or agricultural crops, with LAI > 4 (Baret & Guyot, 1991). The grassland of Val Trupchun would probably have a LAI around 3. Nevertheless, our SRI model still underestimates high biomass. Based on this fact the model was recalculated using two narrow bands, both located in the far RED, as this should solve the saturation problem according to Mutanga and Skidmore (2004). The coefficient of determination (R^2) between band 77 at 765 nm and band 70 at 735 nm is 0.7697, which is only slightly lower than our best SRI (R^2 = 0.7728). On the other hand, the validation yielded 10% better validity (67%). It can be concluded that high biomass values were still underestimated, but at a lower level when avoiding the NIR domain.

5.3 Uncertainty Analysis

The 57% accuracy of the SRI model (842/747) validation means that 57% of the biomass variance can be explained. This is a comparatively good validation for such a complex terrain conducted with completely independent plots. However, several factors showed that the model is relatively instable. The selection of the band combination is one important factor that influences the model accuracy, as illustrated by the example with the narrow band SR index (765/735) in the far RED. The best

calibration should normally result in the best validation. Instead, we found a poorer calibration with a better validation result. This shows that our model alternates and that the sample size is not sufficient enough to develop a robust model. The sample size should be increased.

The selection of the calibration and validation data set also has an influence on the accuracy. We chose the plots belonging to the calibration or the validation data sets completely randomly. Tests with some manual settings, for example implementing the highest and the lowest biomass value into the calibration data set showed that the model output varied. We also tried dividing the double reference points from the different strips, assigning one to the calibration and the other to the validation data sets. However, these model adaptations didn't result in much improvement. The random selection for the calibration and validation data sets was justified and was therefore considered as the best solution. With this number of sample plots (n = 43), higher accuracies are almost impossible to reach. The uncertainties are mainly due to sensitivity to external factors, which overlap the measured signal and influence the model, such as atmospheric effects (cloud, haze and other scatterers), topographic effects (shading), illumination effects (sun angle and viewing geometry), soil effects (soil fraction), structural effects (scattering due to objects/leaf architecture) or random noise. Additionally, the sample itself also has some uncertainty derived from potential sampling inequality and weighting errors.

5.3.1 Different reflectance values between strips

The differences of the APEX data between the overlapping regions of the 4 strips are another point to be discussed. These differences are caused by the variations of illumination- viewing geometry in combination with surface anisotropy. Different parts of an image will view the surface at different angles, so that clear brightness gradients may often be detected across the image (see schema in Figure 27). In fact, the spectral signal reflected from surfaces such as plant canopies is determined by its intrinsic surface anisotropy and consequently varies as a function of the angle of view and the angle of illumination. Shadows are also influenced by different illumination angles. During the pre-calibration of the image, these effects are compensated to the best

possible extent during the basic Bidirectional reflectance distribution function (BRDF) corrections. However, notable differences usually exist as long as no sophisticated BRDF corrections are applied. Therefore, the reflectance of the image pixel of a strip is slightly different from the reflectance of the same pixel available on the neighbouring strip.

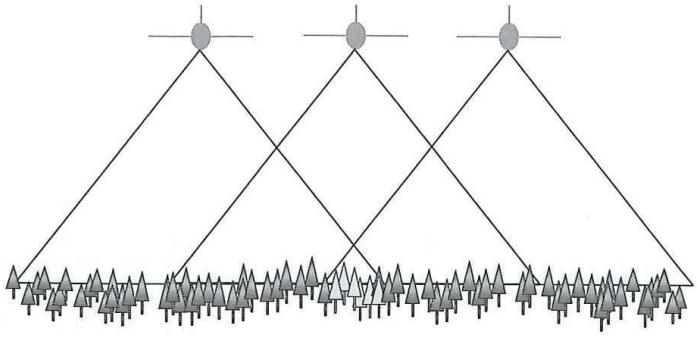

Figure 27: Multiple view angle imaging of vegetation using airborne sensors carried on overlapping flight-paths using wide field-of-view sensors to obtain cross-track data. The highlighted area can be viewed at three different angles (image from Jones & Vaughan, 2010).

We haven't computed any artificial reflectance averaging to obtain one value per image pixel for the overlapping regions. A possibility would have been to build a mosaic of all four strips implementing the reflectance average or favouring one strip. However, each manual computation also involves uncertainties and needs to be justified. It was also not possible to take a single reflectance value from one strip, since we did not record the exact clipping time of every plot. We therefore cannot tell which of the strips correspond better to the biomass data measured. Therefore we decided not to carry out such an artificial intervention with the APEX data and keep all original values from the two strips as independent data.

The scatter plot showed a coefficient of determination R^2 of 0.96 for our optimal SRI (842/727) and 0.95 for the narrow band index (765/735) respectively. Several studies showed that using a narrow band combination in RED is less sensitive to varying soil brightness, atmospheric condition and sensor view angle compared to a broad band combination (Blackburn & Pitman, 1999). With this example this assumption can't be confirmed. Our band selection for the optimal SRI is evidently enough narrow to keep this effect small.

The quantification of these differences with respect to the biomass prediction showed a mean error of 12% for the biomass concentration on the plots. Investigating the individual plots, the highest differences occurred at plot AX16 (32%), AX06 (22%), AX17 and AX14 (both ca. 20%). AX06 is located at Alp Purcher, where the alp hut is located close to the plot. This location is therefore suboptimal and the source of error could derive from scattering from the building to this plot. Plots AX16, AX17 and AX14 are all located on the southern gradient. This area is very steep, the soil is comparatively stony and patches of bare soil are frequent, which are all well known sources of error. (cf. Table 5, Appendix B.)

5.3.2 VARIABILITY OF SAMPLE PLOT LOCATION

Another source of uncertainty in the model is the accuracy of the APEX pixel. In the field, we tried to choose homogeneous plots of 6x6 m and sampled a $1m^2$ subplot in the middle of each plot. Firstly, it was difficult to find homogenous vegetation in the terrain and this is therefore a subjective aspect. Secondly, APEX image spectrometer also has an uncertainty of about 1 pixel (2x2 m), according to RSL. To correlate the biomass sample data with APEX pixel data, we selected 3x3 pixels around the coordinate mid point of each plot. In theory, this corresponds exactly to the 6x6 m of the plots with the clipped square-meter lying in the centre. The reason for taking 3x3 pixels instead of 1 was the following: The overlay of the sample plot coordinates into the APEX image can also involve a maximum mismatch of 1 pixel if the centre coordinates falls on a cell boundary. Another small shift is caused by the plot orientation. Our plots are oriented in direction to the slope and not to the north, as the APEX image is. Therefore, the average reflectance value of the 9 pixels was taken as the reference value.

In Figure 28 two examples of a plot overlain by the APEX image can be seen with the pixel selection indicated. It is visible that the pixel selection for plot AX09 has a small shift because of the different orientation.

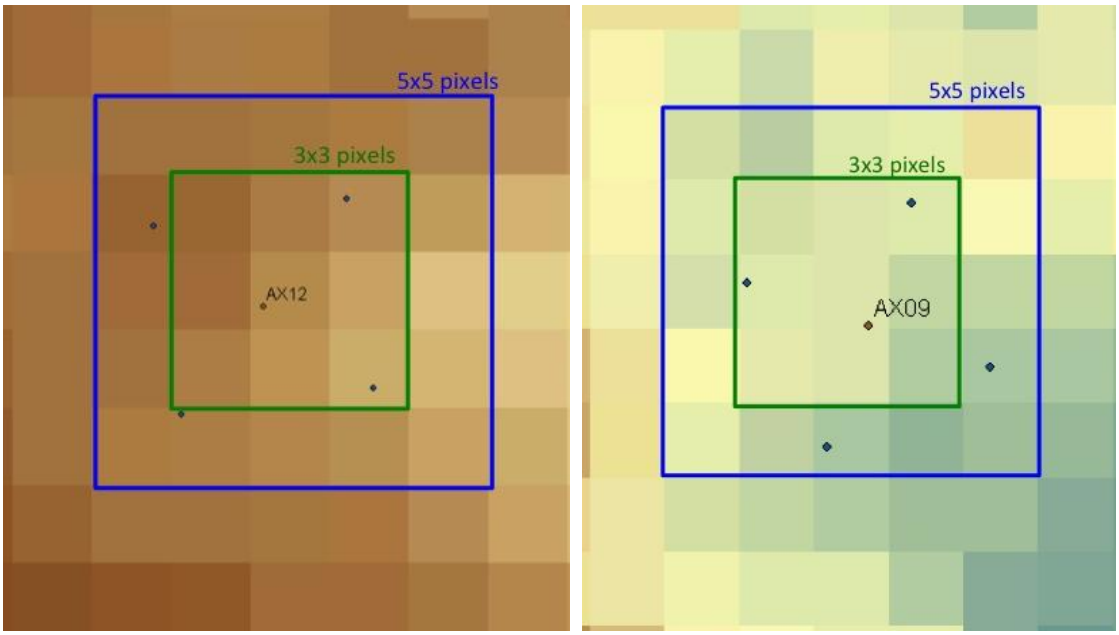

Figure 28: Schematic of plot AX12 (left) and AX09 (right) overlain by the APEX image. The APEX image is oriented in a northerly direction, whereas the plots have been measured in direction to the slope. The dots indicate the true mid points and the corners of the plot, respectively, the green square indicates the 3x3 APEX pixels, the blue square the 5x5 APEX pixel implemented for modelling.

The comparison between average reflectance of 5x5 pixels (10x10 m) and 3x3 pixels (6x6 m) demonstrated how much influence small-scale offsets have and if our plots can be considered as homogenous. The absolute mean difference between the implementation of 3x3 pixels and the 5x5 pixels was 4.6%. We conclude that this is negligible compared to the 57% of total model accuracy. This means that our model, implemented from the average 3x3 pixels as a reference value, is a justified choice and that plots can be generally considered as homogenous. However, the discrepancy between plots AX07 and AX16 is more than 20% (cf. Figure 26). AX07 (entrance to Val Müschauns) is a plot with very high biomass occurrence and is one of the outliers in the model; on the other hand, AX16 (southern gradient) contains very little biomass and is located on a steep slope. A small modification in reflectance might induce a larger effect on the biomass prediction there.

6 CONCLUSION

Imaging spectroscopy techniques permit not only the classification of vegetation, but also the quantitative mapping of different vegetation variables due to their high spectral and spatial resolution. This study demonstrates the utility of vegetation indices involving APEX bands for estimating biomass in alpine grasslands.

SRI and NDVI models were suitable for the modelling of biomass prediction maps implementing biophysical parameters. We found that the correlation between biomass *insitu* measurements and SRIs was non-linear, most likely due to sensor saturation. Our optimal SRI improved the model quality compared to a standard NDVI model. All computed models underestimated high biomass values above 600 g/m^2. The model accuracy of 57% was good considering the challenging terrain. However, several factors showed that the model was relatively unstable due to parameter input settings and external factors. Differences in APEX data between strips induced an important effect, due to different illumination/view angles. The quantification regarding biomass prediction due to these differences produced a mean error of 12% for the sample plots. The variability analysis investigating the sample plot location demonstrated that small-scale geometrical shifts were insignificant compared to the overall model accuracy.

The biomass prediction map showed plausible values for the grassland with high concentrations around the former Alp Trupchun, Alp Purcher and on the south slope at the end of the valley. We found that high biomass sources were linked to former anthropogenic land use, dominant vegetation structure and to preferred ungulate habitat today.

The high-resolution map is now a useful basis for future research in the SNP to investigate forage amount and analyse ungulate habitat pattern in Val Trupchun.

7 OUTLOOK

The generated biomass prediction map can be used for future research in Val Trupchun. This work was carried out within the scope of a PhD thesis at the Swiss National Park analysing ungulate habitat patterns relating to biophysical and biochemical parameters. The APEX campaigns have been continued during the years 2011 and 2012.

The model produced is applicable only for the study area, since semi-empirical. These predictive models are site- and sensor-specific and unsuitable for application to other areas or to different seasons. With this model we tried to predict another area of the SNP, the grassland of Il Fuorn, which is located ca. 15 km north-east, and didn't find suitable agreement with *insitu* measurements. This finding highlights the importance of local models, based on local measurements for small scales in complex terrain.

Moreover, our model is only valid for the time of the image, which was June. To analyse temporal changes for biomass, the APEX campaign should be carried out several times a year.

The main proposal for a model improvement based on this work is to increase the number of sample plots in the study area. With more samples covering the full range of biomass concentrations, we suppose that the model accuracy and stability will improve. Another possibility would be to clip more than 1 m^2 per sample plot to get more than one sample out of one plot. Thus, small-scale variability could be improved, too. However, all improvement proposals would require a lot more effort in the field which is a limiting factor.

For the APEX campaign carried out in June 2012, 100 sample plots have been implemented. Modelling results aren't available yet, we are curious!

8 LIST OF REFERENCES

Achermann, G., Schütz, M., Krüsi, B. O., 2000. Tall-herb communities in the Swiss National Park: Long-term development of the vegetation. Nationalpark-Forschung in der Schweiz, Band 89.

Baret, F., Guyot, G., 1991. Potentials and limits of vegetation indices for LAI and APAR assessment. Remote Sensing of Environment, 35, pp. 161-173.

Beeri, O., Phillips, R., Hendrickson, J., Frank, A. B., Kronberg, S., 2007. Estimating forage quantity and quality using aerial hyperspectral imagery for northern mixed-grass prairie. Remote Sensing of Environment, 110, pp. 216-225.

Birth, G. S., McVey, G. R., 1968. Measuring the colour of growing turf with a reflectance spectrophotometer. Agronomy Journal 60, pp 640-643.

Blackburn, G. A., Pitman, J. I., 1999. Biophysical controls on the directional spectral reflectance properties of bracken (Pteridium aquilinum) canopies: results of a field experiment. International Journal of Remote Sensing, 20(11), pp. 2265-2282.

Boardman, J. W., 1989. Inversion of imaging spectrometry data using singular value decomposition: Proceedings, IGARSS'89, 12th Canadian Symposium on Remote Sensing 4, pp. 2069-2072.

Boschetti, M., Bocchi, S., Brivio, P. A., 2007. Assessment of pasture production in the Italian Alps using spectrometric and remote sensing information. Agriculture, Ecosystems Environment, 118(1-4), pp. 267-272.

Braun-Blanquet, J., Brunies, S., Campell, K., Frey, E., Jenny, H., Meylan, Cli. & Pallmann, H., 1931. Vegetationsentwicklung im Schweiz. Nationalpark. Ergebnisse der Untersuchung von Dauerbeobachtungsflächen, 1. Dokumente zur Untersuchung des Schweizer Nationalparks. Jahresberichte der Nationalforschenden Gesellschaft Graubündens, 69, pp. 3-82.

Braun-Blanquet, J., Pallmann, H., Bach, R., 1954. Planzensoziologische und bodenkundliche Untersuchungen im Schweizerischen Nationalpark und seinen Nachbargebieten. II Vegetation und Böden der Wald- und Zwergstrauch-gesellschaften (Vaccinio-Piceetalia). Ergebnisse der wissenschaftlichen Untersuchungen des schweizerischen Nationalparks. Band 4, Kapitel 28.

Cho, M. A., Skidmore, A., Corsi, F., van Wieren, S. E., Sobhan, I., 2007. Estimation of green grass/herb biomass from airborne hyperspectral imagery using spectral indices and partial least squares regression. International Journal of Applied Earth Observation and Geoinformation 9, pp. 414-424.

Clevers, J. G. P. W., 1999. The use of imaging spectrometry for agricultural applications. ISPRS Journal of Photogrammetry and Remote Sensing 54 (5), pp. 299-304.

Damm, A., Kneubühler, M., Schaepman, M. E., Rascher, U., 2012. Evaluation of gross primary production (GPP) variability over several ecosystems in Switzerland using sun-induced chlorophyll fluorescence derived from APEX data. Proc, IGARSS 2012, Munich (D), July 22-27 2012, pp. 7133-7136.

Falster, D. S, Westoby, M., 2003. Leaf size and angle vary widely across species: what consequences for light interception? New Phytologist 158, pp. 509-525.

Fava, F., Colombo, R., Bocchi, S., Meroni, M., Sitzia, M., Fois, N., Zucca, C., 2009. Identification of hyperspectral vegetation indices for Mediterranean pasture characterization. International Journal of Applied Earth Observation and Geoinformation 11, pp. 233-243.

Geladi, P., Hadjiiski, L., Hopke, P., 1999. Multiple regression for environmental data: nonlinearities and prediction bias. Chemometrics Intell. Lab. Syst. 47 (2), pp 165-173.

Goetz, A. F. H., 2009. Three decades of hyperspectral remote sensing of the Earth: A personal view. Remote Sensing of Environment, 113 (Supplement 1), pp. S5–S16.

Goetz, A. F. H., Vane, G., Solomon, J., & Rock, B. N., 1985. Imaging spectrometry for Earth remote sensing. Science, 228, pp. 1147−1153.

He, Y., Guo, X.L., Wilmshurst, J., 2006. Studying mixed grassland ecosystems I: suitable hyperspectral vegetation indices. Canadian Journal of Remote Sensing 32, pp. 98-107.

Itten, K., Dell'Endice, F., Hueni, A., Kneubühler, M., Schläpfer, D., Odermatt, D., Seidel, F., Huber, S., Schopfer, J., Kellenberger, T., Bühler, Y., D'Odorico, P., Nieke, J., Alberti, E., Meuleman, K., 2008. Sensors 8, pp. 6235-6259.

Jago, R. A., Cutler, M. E. J., Curran, P. J., 1999. Estimating Canopy Chlorophyll Concentration from Field and Airbonre Spectra. Remote Sensing of Environment 68, pp. 217-224.

Jehle, M., Hueni, A., Damm, A., D'Odorico, P., Weyermann, J., Kneubühler, M., Schläpfer, D., Schaepman, M. E., 2010. APEX - current status, performance and product generation. IEEE Sensors 2010, Waikoloa (HI), pp. 533-537.

Jones, H. G., Vaughan, R. A., 2010. Remote sensing of vegetation. Principles, Techniques, and applications. Oxford University Press Inc, New York.

Kneubühler, M., Damm, A., Mundava, Ch., Weyermann, J., Hueni, A., Risch, A. C., Schütz, M., Schweiger, A., Haller, R., Filli, F., Schaepman, M. E., 2011. Imaging Spectrometry for Ecological Studies in a High Mountain Environment. In EARSeL 7th SIG-Imaging Spectroscopy Workshop, Edinburgh, Scotland, 11-13 April.

Kooistra, L., Suarez Barranco, M. D., van Dobben, H. & Schaepman, M. E., 2006. Monitoring Vegetation Biomass in River Floodplains using Imaging Spectroscopy. ISPRS Mid Term Symposium: From Pixels to Processes, Enschede (NL), Kerle, N. & Skidmore, A. (Eds.), ISPRS, p. 5, CD-ROM.

Krüsi, B. O., Schütz, M., Wildi, O., Grömiger, H., 1995. Huftiere, Vegetationsdynamik und botanische Vielfalt im Nationalpark. Cratschla 32, pp 12-25.

Kumar, L., Schmidt, K. S., Dury, S., Skidmore A. K., 2001. Review of hyperspectral remote sensing and vegetation Science. In: Van der Meer, F.D., De Jong, S.M. (eds) Imaging spectrometry: basic principles and prospective applications. Kluwer, Dordrecht, The Netherlands.

Liang, S., 2004. Quantitative remote sensing of land surfaces. Hoboken: Wiley, Hoboken.

Lillesand, T. M., Kiefer, R. W., 1994. Remote sensing and image interpretation, 3rd ed. New York: John Wiley and Sons, Inc.

Mirik, M., Norland, J. E., Crabtree, R. L., and Biondini, M. E., 2005a. Hyperspectral one-meter-resolution remote sensing in Yellowstone National Park, Wyoming: I. Forage nutritional values. Rangeland Ecology and Management 58, pp. 452-458.

Mirik, M., Norland, J. E., Crabtree, R. L., Biondini, M. E., 2005b. Hyperspectral one-meter-resolution remote sensing in Yellowstone National Park, Wyoming: II. Biomass. Rangeland Ecology and Management 58, pp. 459-465.

Mutanga, O., Skidmore, A. K., 2004. Integrating imaging spectroscopy and neural networks to map grass quality in the Kruger National Park, South Africa. Remote Sensing of Environment 90, pp. 104-115.

Mutanga, O., Skidmore, A. K., 2004. Narrow band vegetation indices overcome the saturation problem in biomass estimation. International Journal of Remote Sensing, Vol. 25, pp. 3999-4014.

Mutanga, O., Skidmore, A. K., 2007. Red edge shift and biochemical content in grass canopies. ISPRS Journal of Photogrammetry and Remote Sensing 62, pp. 34-42.

Mutanga, O., Skidmore, A. K., Prins, H. H. T., 2004. Predicting in situ pasture quality in the Kruger National Park, South Africa, using continuum-removed absorption features. Remote Sensing of Environment, 89, pp. 393-408.

Numata, I., Roberts, D. A., Chadwick, O. A., Schimel, J., Galvao, J., Soares, J. V., 2008. Evaluation of hyperspectral data for pasture estimate in the Brazilian Amazon using field and imaging spectrometers. Remote Sensing of Environment, 112, pp. 1569-1583.

Numata, I., Roberts, D. A., Chadwick, O. A., Schimel, J., Sampaio, F. R., Leonidas, F. C., Soares, J. V., 2007. Characterization of pasture biophysical properties and the impact of grazing intensity using remotely sensed data. Remote Sensing of Environment, 109, pp. 314-327.

Parolini, J. D., 1995. Zur Geschichte der Waldnutzung im Gebiet des Schweizerischen Nationalparks. PhD Thesis ETH Zurich, Nr. 1187.

Pictet, A., 1942. Les Macrolépidoptères du parc national Suisse et des régions limitrophes. Ergebnisse der wissenschaftlichen Untersuchungen des schweizerischen Nationalparks. Band 1, Kapitel 8.

Psomas, A., 2009. Hyperspectral remote sensing for ecological analyses of grasslands ecosystems. Spectral separability and derivation of NPP related biophysical and biochemical parameters. Dissertation, University of Zurich.

Rahman A. F., Gamon J. A., 2004. Detecting biophysical properties of a semi-arid grassland and distinguishing burned from unburned areas with hyperspectral reflectance. Journal of Arid Environments 58(4), pp. 597-610.

Rosso, P. H., Ustin, S. L., Hastings, A., 2005. Mapping marshland vegetation of San Francisco Bay, California, using hyperspectral data. Int. Journal of Remote Sensing, Vol. 26, Nr. 23, pp. 5169-5191.

Rouse, J. W., Haas, R. H., Schell, J. A., Deering, D. W., Harlan, J C., 1974. Monitoring the vernal advancement and retrogradation (greenwave effect) of natural vegetation. NASA/GSFC Final report, Greenbelt, MD, USA.

Schaepman, M., Schläpfer, D., Kaiser, J., Brazile, J., Itten, K., 2003. APEX-Airborne Prism Experiment: Dispersive Pushbroom Imaging Spectrometer for Environmental Monitoring. 3rd EARSeL Workshop on Imaging Spectroscopy, Proc. CD_ROM.

Schläpfer, D., Richter, R., 2002. Geo-atmospheric processing of airborne imaging spectrometry data. Part 1: parametric orthorectification. International Journal of Remote Sensing, Vol. 23, pp. 2609-2630.

Stessens, J., 2012. BruHyp 2012, conference slides, p. 24.

Stüssi, B., 1970. Naturbedingte Entwicklung subalpiner Weiderasen auf Alp La Schera im Schweizer Nationalpark während der Reservatsperiode 1939-1965. Ergebnisse der wissenschaftlichen Untersuchungen im schweizerischen Nationalpark, 13.

Tarr, A. B., Moore, K. J., Dixon, P. M., 2005. Spectral reflectance as a covariate for estimating pasture productivity and composition. Crop Science, 45(3), pp. 996-1003.

Trepp, W., Campell, E., 1968. Vegetationskarte des Schweizerischen Nationalpark. Nationalparkforschung in der Schweiz, Band 11, Heft 58

Tucker, C. J., 1979. Red and photographic infrared linear combinations for monitoring vegetation. Remote Sensing of Environment 8, pp 127-150.

Vane, G., Chrisp, M., Emmark, H., Macenka, S., Solomon, J., 1984. Airborne Visible Infrared Imaging Spectrometer (AVIRIS): An Advanced Tool for Earth Remote Sensing. European Space Agency. Special Publication, ESA SP, 2, 751.

Van Langevelde, F., Prins, H. H. T., 2008. Introduction to resource ecology. In Prins, H. H. T., and Van Langevelde, F. (eds.). Resource Ecology, Spatial and Temporal Dynamics of Foraging. Springer, Dordrecht, pp 1-6.

Weyermann, J., Damm, A., Kneubühler, M., Schaepman, M. E., 2013. Correction of reflectance anisotropy effects of vegetation on airborne spectroscopy data and derived products. IEEE Transactions on Geosciences and Remote Sensing.

Xiao, Q., Ustin, S. L., McPherson, E. G., 2004. AVRIS data and mulitple-masking techniques to map urban tree species. International Journal of Remote Sensing, Vol. 25, No. 24, pp. 5637-5654.

Zoller, H., 1992. Vegetationskarte des Schweizerischen Nationalparks und seiner Umgebung. Nationalpark-Forschung in der Schweiz, Band 85.

Campbell, G. S., Norman, J. M., 1998. An introduction to environmental biophysics. 2nd ed., Springer, New York, pp. 286.

9 GLOSSARY

AISA	Airborne Imaging Spectrometer for Applications
APEX	Airborne Prism Experiment
AVIRIS	Airborne Visible/Infrared Imaging Spectrometer
asl	above sea level
BDRF	Bidirectional reflectance distribution function
CHB	Calibration home base
CSU	Control and storage unit
DLR	Deutsches Zentrum für Luft- und Raumfahrt
ENVI	Environment for Visualisation of Images
ESA	European Space Agency
FOV	Field of view
FWHM	Full width at half maximum
GIS	Geographic Information System
GPS	Global Positioning System
GREEN	Green part of the electromagnetic spectrum
HABITALP	Alpine Habitalp Diversity project
HCRF	Hemispherical-conical-reflectance
HyMAP	Hyperspectral Mapper
IDL	Interactive Data Language
IFOV	Instantenous field of view
IUCN	International Union for the Conservation of Nature
LAI	Leaf Area index
LSU	Linear spectral unmixing method
MODIS	Moderate-resolution Imaging Spectroradiometer
NASA	National Aeronatics and Space Administration
NDVI	Normalized Differenced Vegetation index
NIR	Near infrared part of the electromagnetic spectrum
NPV	Non-photosynthetic active vegetation
PAF	Processing and archiving facility
PV	Photosynthetically active
RED	Red part of the electromagnetic spectrum
REPI	Red edge position index
RMSE	Root mean square error
RSL	Remote Sensing Laboratroy, University of Zurich
SD	Standard deviation
SNP	Swiss National Park
SNP	Signal-to-noise
SRI	Simple Ratio index
SWIR	Shortwave infrared part of the electromagnetic spectrum
VI	Vegetation index

VIS	Visible part of the electromagnetic spectrum
VITO	Vision on Technology

10 APPENDIX

A) DETAILED MAP OF SAMPLE PLOT LOCATIONS

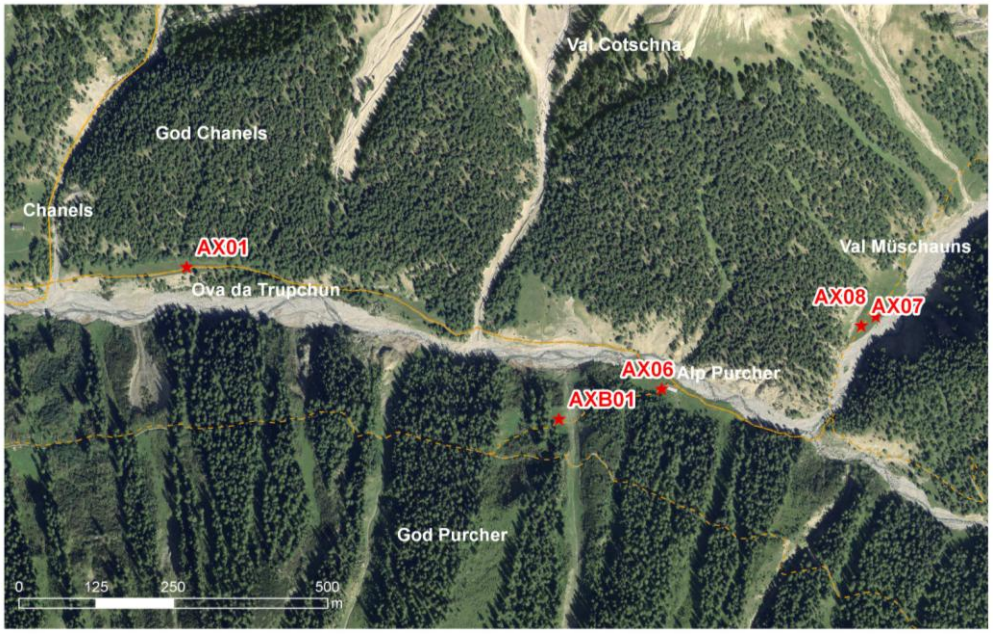

Figure 29: Map of the entrance of Val Trupchun with plots AX101, AX06, AXB01, AX06 and AX07 indicated

Figure 30: Detailed map of the middle part of Val Trupchun, Dschembrina, God Malgöletta and God Trupchun with AXF02, AXB02, AXB03, AXB04 and AXB05 indicated

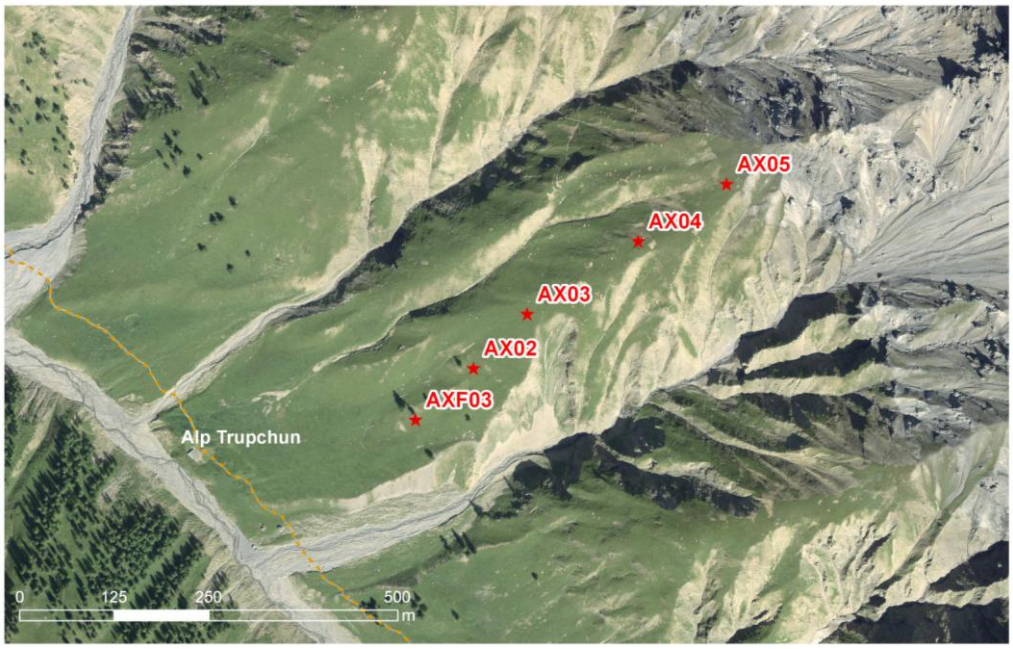

Figure 31: Map of the Alp Trupchun and the north slope of the valley with plot AXF03, AX02, AX03, AX04 and AX05

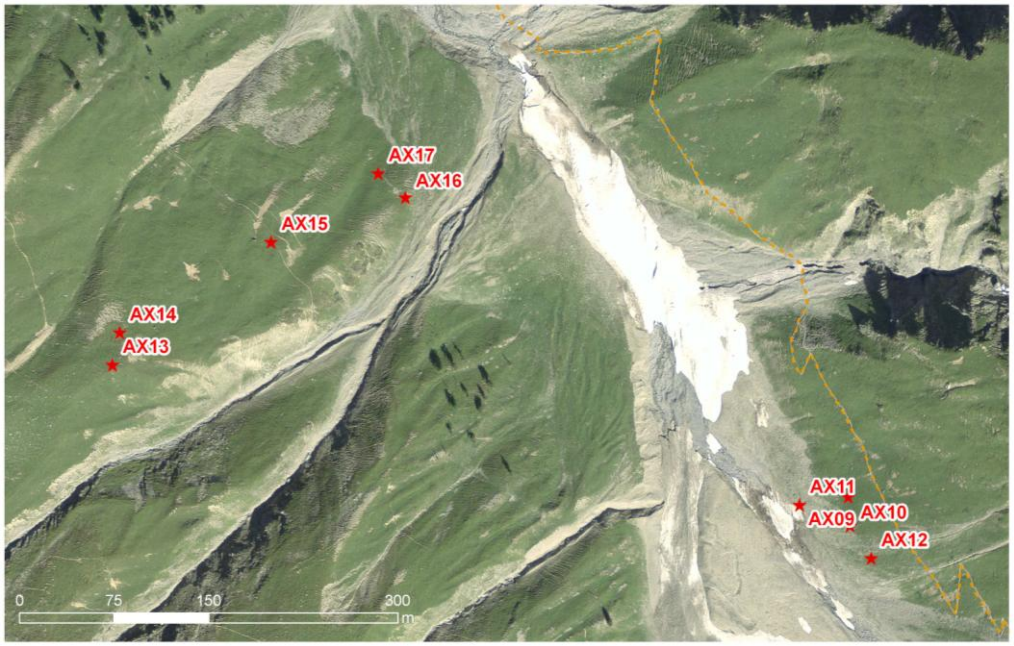

Figure 32: Map of the inner most part of the valley and the south slope of the valley with plots indicated

B) MODEL RESULTS

Table 3: Overview of the calibration and validation data set selection (random)

Plot	Data Set	
	Calibration	*Validation*
1	AX01_S72	AX16_S42
2	AX04_S52	AX17_S42
3	AX07_S62	AX02_S52
4	AX09_S42	AX03_S52
5	AX09_S52	AX05_S52
6	AX10_S42	AX10_S10
7	AX11_S42	AX13_S52
8	AX11_S52	AX14_S52
9	AX12_S42	AX17_S52
10	AX12_S52	AXB02_S52
11	AX13_S42	AXB03_S52
12	AX14_S42	AXB05_S52
13	AX15_S42	AXF02_S52
14	AX15_S52	AXF03_S52
15	AX16_S52	AX06_S62
16	AXB01_S72	AX08_S62
17	AXB03_S62	AXB01_S62
18	AXB04_S52	AXB02_S62
19	AXB04_S62	AX06_S72
20	AXB05_S62	AX07_S72
21	AXF01_S62	AX08_S72
22	AXF02_S62	

Table 4: Correlation hotspots with R > 0.8 from 2D contour plot

	Bands	
Region	*i*	*j*
1	546 - 585	694 - 727
2	540 - 552	820 - 879
3	540 - 585	932 - 1289
4	723 - 743	765 - 860
5	1298 - 1308	1558 - 1672
6	1175 - 1308	1733 - 1768
7	1069 - 1308	2391 - 2432

Table 5: Calculation results of different reflectance values between stripes and effect on biomass prediction

Plot	SRI stripe a	SRI stripe b	Biomass a [g/m^2]	Biomass b [g/m^2]	Difference biom. [g/m^2]	Difference [%]
AX06	0.8895	0.8948	667.2	679.8	12.6	1.9
AX07	0.8134	0.8161	510.2	515.1	4.8	0.9
AX08	0.7794	0.8116	452.6	507.1	54.4	10.7
AX09	0.7781	0.7182	450.7	364.9	-85.7	-23.5
AX10	0.2638	0.2881	73.6	80.2	6.6	8.2
AX11	0.1103	0.1427	42.9	48.1	5.2	10.8
AX12	0.3784	0.3700	110.2	107.0	-3.2	-3.0
AX13	0.7548	0.7488	415.1	406.4	-8.7	-2.1
AX14	0.5649	0.5744	212.6	219.9	7.2	3.3
AX15	0.7830	0.7798	458.4	453.4	-5.0	-1.1
AX16	0.3930	0.4948	116.1	166.1	50.1	30.1
AX17	0.6224	0.6899	260.4	330.3	69.9	21.2
AXB01	0.8581	0.8479	597.3	576.2	-21.1	-3.7
AXB02	0.6916	0.7283	332.2	378.0	45.8	12.1
AXB03	0.6519	0.6921	288.9	332.8	43.9	13.2
AXB04	0.5722	0.6546	218.1	291.7	73.6	25.2
AXB05	0.8366	0.7820	553.7	456.9	-96.8	-21.2
AXF02	0.6933	0.7158	334.2	361.8	27.6	7.6
					absolute mean	11.1